CANCER GENOMICS & PROTEOMICS *17*: 469-497 (2020)
doi:10.21873/cgp.20205

Whole-transcriptome Analysis of Fully Viable Energy Efficient Glycolytic-null Cancer Cells Established by Double Genetic Knockout of Lactate Dehydrogenase A/B or Glucose-6-Phosphate Isomerase

ELIZABETH MAZZIO[1], RAMESH BADISA[1], NZINGA MACK[1], SHAMIR CASSIM[2], MASA ZDRALEVIC[3#], JACQUES POUYSSEGUR[2,3] and KARAM F.A. SOLIMAN[1]

[1]*College of Pharmacy & Pharmaceutical Sciences, Florida A&M University, Tallahassee, FL, U.S.A.;*
[2]*Department of Medical Biology, Centre Scientifique de Monaco, Monaco, Monaco;*
[3]*University Côte d'Azur, IRCAN, CNRS, Centre A. Lacassagne, Nice, France*

Abstract. *Background/Aim: Nearly all mammalian tumors of diverse tissues are believed to be dependent on fermentative glycolysis, marked by elevated production of lactic acid and expression of glycolytic enzymes, most notably lactic acid dehydrogenase (LDH). Therefore, there has been significant interest in developing chemotherapy drugs that selectively target various isoforms of the LDH enzyme. However, considerable questions remain as to the consequences of biological ablation of LDH or upstream targeting of the glycolytic pathway. Materials and Methods: In this study, we explore the biochemical and whole transcriptomic effects of CRISPR-Cas9 gene knockout (KO) of lactate dehydrogenases A and B [LDHA/B double KO (DKO)] and glucose-6-phosphate isomerase (GPI KO) in the human colon cancer cell line LS174T, using Affymetrix 2.1 ST arrays. Results: The metabolic biochemical profiles corroborate that relative to wild type (WT), LDHA/B DKO produced no lactic acid, (GPI KO) produced minimal lactic acid and both KOs displayed higher mitochondrial respiration, and minimal use of glucose with no loss of cell viability. These findings show a high biochemical energy efficiency as measured by ATP in glycolysis-null cells. Next, transcriptomic analysis conducted on 48,226 mRNA transcripts reflect 273 differentially expressed genes (DEGS) in the GPI KO clone set, 193 DEGS in the LDHA/B DKO clone set with 47 DEGs common to both KO clones. Glycolytic-null cells reflect up-regulation in gene transcripts typically associated with nutrient deprivation / fasting and possible use of fats for energy: thioredoxin interacting protein (TXNIP), mitochondrial 3-hydroxy-3-methylglutaryl-CoA synthase 2 (HMGCS2), PPARγ coactivator 1α (PGC-1α), and acetyl-CoA acyltransferase 2 (ACAA2). Other changes in non-ergometric transcripts in both KOs show losses in "stemness", WNT signaling pathway, chemo/radiation resistance, retinoic acid synthesis, drug detoxification, androgen/estrogen activation, and extracellular matrix reprogramming genes. Conclusion: These findings demonstrate that: 1) The "Warburg effect" is dispensable, 2) loss of the LDHAB gene is not only inconsequential to viability but fosters greater mitochondrial energy, and 3) drugs that target LDHA/B are likely to be ineffective without a plausible combination second drug target.*

[#]Present address: Faculty of Medicine, University of Montenegro, Kruševac bb, 81000 Podgorica, Montenegro.

Correspondence to: Karam F.A. Soliman, Room G 134 H New Pharmacy Building, 1415 ML King Blvd, Tallahassee, FL 32307, U.S.A. Tel: +1 8505993306, e-mail: karam.soliman@famu.edu; Jacques Pouyssegur, Centre Scientifique de Monaco, CSM, 98000 Monaco, Monaco. E-mail: Jacques.pouyssegur@unice.fr

Key Words: Cancer, metabolism, LDHA, LDHB, GPI, Warburg effect, genes.

Common features across diverse mammalian tumors include the rapid glycolytic activity, greater expression of lactate dehydrogenases (LDH) and subsequent over-production of lactic acid, occurring regardless of the presence of oxygen (Warburg effect) (1,2). This unique trait of cancer has been studied for decades, where researchers have geared off original focus from its role in metabolism to its role in acidification of the tumor microenvironment (TME), a formidable driving force for tumor growth, metastasis, aggressiveness, chemo/radiation resistance and loss of immune surveillance (3-8). This loss of immune surveillance

involves a concurrent loss of host T and NK cell functions combined with tumor sequestration of immune leukocyte subpopulations, infiltrated in solid acidic tumors, promoting tumor survival (7, 9). TME acidification directly correlates to tumor progression, which has been exploited pharmacologically for the development of drug delivery systems such as low pH insertion peptides pHLIP (10, 11), or delivery diagnostic tools (12), while attempts at reducing acidity genetically or by pharmacological means include drugs that target LDHA and lactate/H^+ symporters (13).

Previously, our laboratory conducted a high throughput screening of over a thousand natural herbs and phytochemicals for inhibition of LDHA (14). LDHA inhibitors, once identified, were then evaluated for their effects on metabolic parameters in MDA-MB-231 breast cancer cells, showing no cell death or reduced production of lactic acid, with the only observable effects being the reduction in proliferative rate (15). Subsequently, we silenced the *LDHA* gene in MDA-MB-231 cells, where we again reconfirm no adverse consequential effects on viability, lactic acid, energy, or any other observable malignant attribute (16). Subsequent studies led us to investigate all LDH isoforms in this particular cell line – revealing a high dominance of co-existent LDHA and B. We suggested that a double knockdown would be required to reduce both *LDHA*/*B* gene expressions to accurately identify the consequences to the loss of this gene. At the same time, Pouyssegur's research group created dual (*LDHA*/*B*) knock out clones using CRISPR-Cas9 genome editing, where they reported that this double genetic disruption completely eliminated lactic acid production in human colon adenocarcinoma (LS174T) and mouse melanoma (B16) cells, having no effect on viability, yet coinciding with greater mitochondrial OXPHOS capacity (17, 18). They also established a clone with complete genetic ablation of *glucose-6-phosphate isomerase* (GPI), which, similarly to the *LDHA*/*B* DKO, showed reduced lactic acid production, greater reliance on OXPHOS and suppressed growth in hypoxia (18-20).

Given the unusual survival of tumor cells in response to the severe compromise of glycolysis, in this work we used Affymetrix whole-transcriptome microarrays combined with metabolic biochemical evaluation to explore survival mechanisms.

Materials and Methods

Materials. Ninety-six well plates, pipette tips, Dulbecco's modified Eagle's medium (DMEM), fetal bovine serum (FBS), penicillin/streptomycin, general reagents and supplies were all purchased from Sigma-Aldrich Co. (St. Louis, MO, USA) and VWR International (Radnor, PA, USA). All microarray equipment, reagents, and materials were purchased from Affymetrix/ Thermo Fisher (Waltham, MA, USA).

Cell culture. Dukes' type B, colorectal adenocarcinoma LS174T (ATCC® CL-188™) WT *versus GPI* KO and *LDHA*/*B* double KO (DKO) were established and provided by Dr. Pouyssegur's lab (17, 18). The cells were cultured in 75 cm^2 flasks containing high glucose DMEM supplemented with 6% FBS and 1% 10,000 U/ml penicillin G sodium/10,000 μg/ml streptomycin sulfate. Cells were grown at 37˚C in 95% atmosphere 5% CO_2 and sub-cultured every three to five days. The WT control grew in multi-cellular aggregates, which required trypsin detachment [Trypsin-EDTA (0.25%), phenol red] on a regular basis through pressurized distribution using a 5 ml serological pipette, deactivation with FBS growth media, and monolayer re-seeding. Both KO clones grew in relatively well-distributed monolayers. High glucose DMEM (4,500 mg/l) was used for all studies, except for monitoring glucose consumption, which required low glucose DMEM (1000 mg/l) to unmask differential rates between the three clones.

Cell viability. Cells were equally plated in 96 well plates at 5×10^5 cells/ml in high glucose media. The resazurin (alamar blue) indicator dye was used to measure viability (21). Briefly, a working solution of resazurin (0.5 mg/ml) was prepared in sterile PBS and filter sterilized through a 0.2-micron filter. The dye solution was added to the samples [15% (v/v) equivalent], and samples were then returned to the incubator for 6-12 h. Reduction of the dye by viable cells reduced the oxidized resazurin, yielding a bright red fluorescent intermediate resorufin quantified using a Synergy HTX multi-mode reader (Bio-Tek, Winooski, VT, USA) with the following settings: 530 nm (excitation)/590 nm (emission) filters.

Lactic acid. Determination of lactic acid produced and released in the media by the three clones was done from cells plated at a density of 5×10^5 cells/ml by dual detection. Lactic acid was quantified by HPLC (Shimadzu), equipped with an SPD-20A UV detector (set at 210 nm), a workstation containing EZSTART version 7.4 software and an SS420X instrument interface docked to a Waters Autosampler Model 717 Plus (Shimadzu Scientific Instruments, Columbia, MD, USA; Waters, Milford, MA, USA). The flow rate was isocratic at 0.6 ml/min. The mobile phase contained 5mM sulfuric acid, and the column used was an Aminex HPX-87H 300×7.8 mm; 9 μm particle size (Bio-Rad, Hercules, CA, USA). Lactic acid was also determined using a colorimetric enzymatic assay using lactate reagent protocol as provided by the manufacturer (Trinity Biotech, Jamestown, NY, USA). The reagent was added to the samples and incubated for 8 minutes. Lactate was quantified at 490 nm using a Synergy HTX multi-mode reader (Bio-Tek). Experimental media for this assay was high glucose DMEM, containing 1% FBS, 4 mM L-glutamine, and penicillin/streptomycin (100 U/0.1 mg/ml) (minus phenol red). Lower FBS was required to carry out the colorimetric assay, as it interferes with the lactate reagent.

Glucose consumption. Briefly, glucose was quantified by an enzymatic assay using glucose oxidase (20 U/ml) and a chromogenic solution, then quantified at 490 nm on the Synergy/HTX multi-mode reader (Bio-Tek). Experimental media for this assay was DMEM (glucose 1000 mg/l) containing 1% FBS, 4 mM L-glutamine and penicillin/streptomycin (100 U/0.1 mg/ml) (minus phenol red).

Somatic cell ATP. Adenosine triphosphate (ATP) was assessed by using the Adenosine 5'-triphosphate (ATP) bioluminescent somatic cell assay kit (Catalog Number FLASC) purchased from Sigma Aldrich (St. Louis, MO, USA) and carried out according to the manufacturer's instructions. Briefly, cells were lysed with ATP releasing reagent, transferred to a flat white bottom 96 well plate and quantified on a Synergy HTX multi-mode reader (Bio-Tek) using luminescence settings.

Oxygen consumption. The oxygraph respirometer-Clark electrode (Hansatech Instruments Ltd., Norfolk, England) was used to evaluate cellular/mitochondrial respiration indirectly by evaluating dissolved O_2 in the media. The electrode was calibrated with both air saturated deionized water and deionized water bubbled with nitrogen for 20 minutes, with additional sodium dithionite to stabilize zero oxygen line calibration. Briefly, the cell supernatants or control media blanks were loaded into the cell chamber jacket at 25˚C. After rate equilibration, a reading was taken, and data were plotted as μM O_2 consumed/ 24 h.

Microarray WT 2.1 human datasets. All cells were washed three times in ice-cold HBSS, rapidly frozen and stored at –80˚C. Total RNA was isolated and purified using the Trizol/chloroform method. The quality was assessed, and concentration was equalized to 82 ng/μl in nuclease-free water. Whole transcriptome analysis was conducted according to the GeneChipTM WT PLUS Reagent Manual for Whole Transcript (WT) Expression Arrays. Briefly, RNA was reverse transcribed to first-strand /second-strand cRNA, cRNA was purified and assessed for yield, prior to the second cycle single-stranded cDNA synthesis, hydrolysis of RNA, and purification of the second cycle single-stranded cDNA. Subsequently, cDNA was assessed for yield, then fragmented, labeled, and hybridized onto the arrays prior to being subjected to fluidics and imaging using the Gene Atlas (Affymetrix, ThermoFisher Scientific). The array data quality control and initial processing from CEL to CHP files were conducted using an expression console, prior to data evaluation using the Affymetrix transcriptome analysis console and String Database (String Consortium 2020) (22, 23). The dataset has been deposited to NIH Gene Expression Omnibus located at: https://www.ncbi.nlm.nih.gov/geo/query/acc.cgi?acc=GSE149289.

Data analysis. Statistical analysis was performed using GraphPad Prism (version 3.0; Graph Pad Software Inc., San Diego, CA, USA) with the significance of difference between the groups assessed using a one-way ANOVA and then followed by Tukey post hoc analysis.

Results

Metabolic profiling. The metabolic parameters in WT and *GPI KO* LS174T as well as *LDHA/B* DKO colon adenocarcinoma cells were acquired at 24h for viability (Figure 1A), cell respiration (Figure 1B), glucose consumption (Figure 1C), lactic acid production/release (Figure 1D) and somatic ATP generation (Figure 1E). The findings clearly suggest that both subset KO LS174T viable clones are capable of maintaining energy to thrive, with the primary difference being that the *GPI* KO and *LDHA/B* DKO clones display impaired glycolytic ability, as evidenced by the severe loss of lactic acid production, occurring to a greater extent in the latter subset (*LDHA/B* DKO). These data also show greater ATP yield in both knockouts compared to the WT, with no detectable levels of glucose being consumed within the first 48 h. Experimental protocols to sufficiently quantify glucose consumption rates required low glucose media (1000 mg/l), with data obtained when controls consumed most of the glucose in 96 well plates with an endpoint at 48 h (Figure 1C). This experimental design clearly shows a difference in the WT controls which utilize glucose at a fairly rapid rate, tantamount to the production of lactic acid. In summary, baseline studies confirm that fermentative glycolysis is not required for cells to maintain energy systems, cells can overcome a complete loss of *LDHA/B* where there appears to be a significant switch to an efficient ATP producing system, non-reliant on glucose. In order to investigate how KO clones overcome a near-complete loss of glycolysis, whole transcriptomic microarrays were then conducted.

Microarray. The overall bio statistical summary data for the microarrays were quantified according to the following analysis set parameters: Fold Change: >2 or <-2, *p*-Value<0.05, and filtered for only characterized genes. The summary analysis report shows 48,226 genes evaluated, 273 deferentially expressed genes (DEGS) were found in the *GPI* KO clone set, 193 DEGS in the *LDHA/B* DKO clone set with 47 DEGs consistent to both KO clones (Figure 2). These changes correspond to transcriptomic shifts being less than 0.5% of the transcriptome affected in both glycolysis-null KOs (Figure 3A, B). Detailed data on the DEGs are presented for both independent clones (Tables I and II) and DEGs consistent to both clones (Table III).

DEG tables. Table I reflects the most significant shift in DEGs for the *LDHA/B* DKO clone set *versus* WT controls, where the highest down-regulated genes were: mucin 6 (*MUC6*), dickkopf (WNT signaling pathway inhibitor) 4 (*DKK4*), alanyl (membrane) aminopeptidase (*ANPEP*), EPS8-like 3 (*EPS8L3*) and solute carrier family 44 member 4 (*SLC44A4*), while the highest up-regulated genes were among others: cilia and flagella associated protein 126 (*CFAP126*), 2-5-oligoadenylate synthetase 2 (*OAS2*), neurotensin (*NTS*) and serine peptidase inhibitor, Kazal type 1 (*SPINK1*).

Table II reflects the most significant shift in DEGs for the *GPI* KO clone set *versus* WT controls, where down-regulated genes show the highest losses for: dickkopf WNT signaling pathway inhibitor 4 (*DKK4)*, gap junction protein alpha 1 (*GJA1*), versican (*VCAN*), biglycan (*BGN*), and the top up-regulated genes were: S100 calcium-binding protein A7 (*S100A7*), v-kit Hardy-Zuckerman 4 feline sarcoma viral oncogene homolog (*KIT*), 5-hydroxytryptamine (serotonin) receptor 1D, G protein-coupled (*HTR1D*) and 3-hydroxy-3-methylglutaryl-CoA synthase 2, which is mitochondrial (*HMGCS2*).

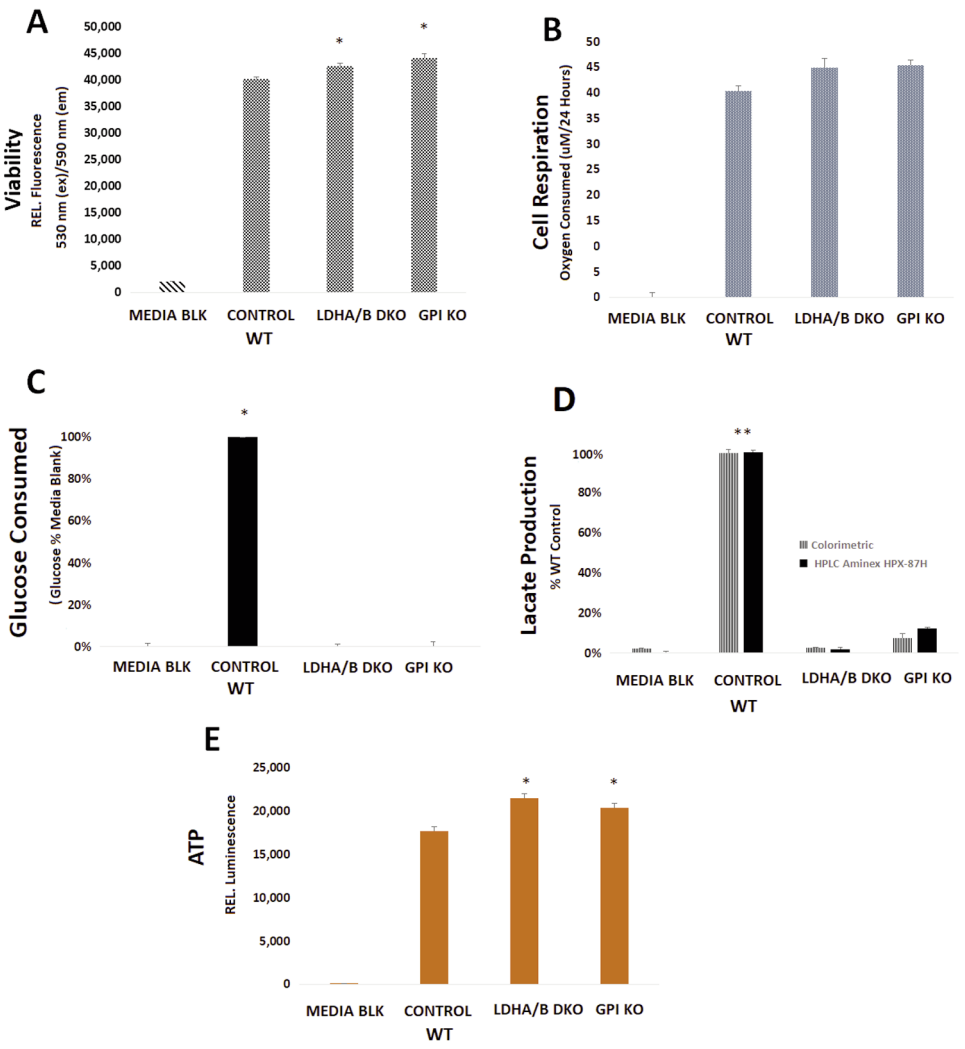

Figure 1. *Metabolic parameters in the control WT (LS174T) cells, relative to LDHA/B double knockout (DKO) and GPI KO including: (A) basic viability [relative fluorescent intensity defined as 530 (ex)/590 (em)], (B) oxygen respiration (O2 consumed μM/ 24 h), (C) glucose consumption (media glucose concentrations as a % of WT controls with no defect in glycolysis), (D) lactic acid production (lactic acid produced as a % of WT controls with no defect in glycolysis) and (E) somatic ATP concentrations (relative luminescent values). The data was analyzed by a one way ANOVA, followed by a Tukey post hock test, where significant differences are represented by *p-Value <0.05 and significant differences established for the following: (A-B) WT versus KO clones, (C) glucose media versus consumption in the 3 clones, (D) lactic acid production in 3 clones versus media blank and (E) WT versus KO clones.*

Table III shows only overlapping unidirectional DEGs for both glycolytic KO clones *versus* WT where down-regulated genes show the most significant losses for: dickkopf WNT signaling pathway inhibitor 4 (*DKK4*), biglycan (*BGN*), desmocollin 3 (*DSC3*), crystallin beta B1(*CRYBB1*), aldo-keto reductase family 1, member C2 (*AKR1C*), aldo-keto reductase family 1, member B10 (aldose reductase) (*AKR1B10*), and calbindin 2 (*CALB2*). The top up-regulated genes included among others: serine peptidase inhibitor (*SPINK1*), Kazal type 1, FXYD domain-containing ion transport regulator 4 (*FXYD4*), 3-hydroxy-3-methylglutaryl-CoA synthase 2 (mitochondrial) (*HMGCS2*), peroxisome proliferator-activated receptor gamma and coactivator 1 alpha (*PPARGC1A*).

Transcriptome analysis console (TAC) pathway analysis. The totality of the microarray data show that many of the DEGs in clone subsets did not fall on known Wiki metabolic pathways. TAC pathway analysis for glycolysis and TCA cycle genes is shown in Figure 4. In the *LDHA/B* DKO clones, the data show very few changes accompanying the loss of LDH transcripts, including a reduction in *phosphofructokinase* (*PFKP*) with a

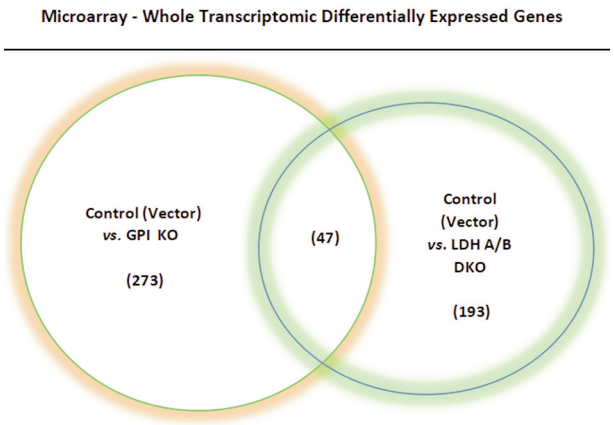

Figure 2. *Whole transcriptome summary of deferentially expressed genes (DEG) in both clones (LDHA/B DKO and GPI KO) vs. WT Vector controls in the LS174T colon cancer cell line, and overlapping genes common to both KO clones. Analysis conditions: fold change >2 or p-Value<0.05. Total number of genes analyzed: 48226. Results: 273 DEGS (GPI KO) and 193 DEGS (LDHA/B DKO) and 47 DEGS common to both KO cell lines.*

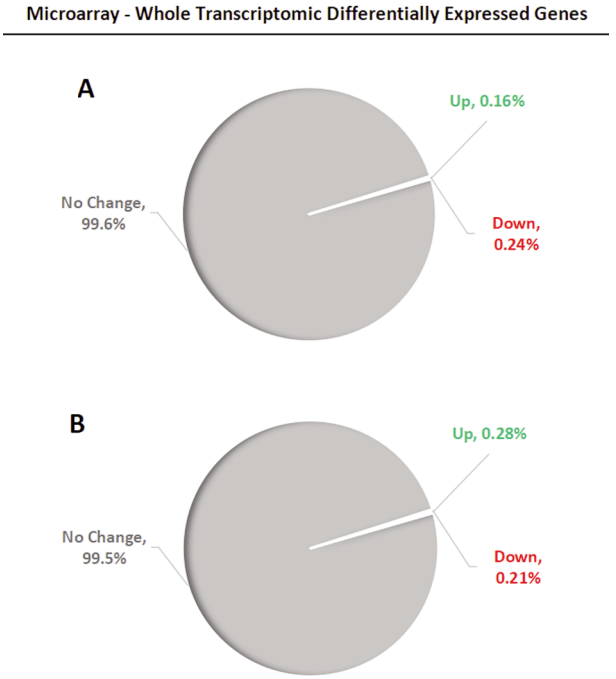

Figure 3. *Whole transcriptome summary of DEGs in both clones (LDHAB DKO) (A) and (GPI KO) (B) versus WT vector controls in the LS174T colon cancer cell lines, with respect to the entire genome, also reflecting % of up and down DEGs in both clones. Analysis conditions: fold change >2 or p-Value<0.05. Total number of genes: 48226. (A) LDHAB DKO: Up-regulated 78 (0.16%) and Down-regulated 115 (0.24%), (B) GPI KO: Up-regulated 84 (0.28%) and Down-regulated 121 (0.21%).*

rise in *phosphoenolpyruvate carboxykinase 1* (*PCK1*), with no modifications to the TCA cycle gene transcripts. The *GPI* KO clone set shows a compensatory increase in *SLC2A1*, *enolase 2* (*ENO2*), *aldolase, fructose-bisphosphate C* (*ALDOC*) and *hexokinase* (*HK2*), with few to no changes in the TCA cycle-related gene transcripts. Integrated pathway analysis (Figure 5A, B) is also provided, which shows potential changes in pyruvate metabolism, glycolysis and gluconeogenesis, urea cycle, glutamate metabolism, ketone bodies, and fatty acid metabolism. Again, these data show very few additional changes in response to severe glycolytic inhibition: *LDHA/B* DKO displays reduction in *argininosuccinate synthase 1* (*ASS1*, urea cycle), *cystathionine gamma lyase* (*CTH*, cysteine metabolism), *aldehyde dehydrogenase 1, family member 1* (*ALDH1A1*, aldehyde metabolism) and significantly elevated expression of *HMGCS2* (Figure 6A), while *GPI* KO reflects a unique elevation in *arginase 2* (*ARG2*, urea cycle). The prominent overlapping transcriptomic shifts consistent in both clone subsets involve the rise in expression of *HMGCS2* in the HMG-CoA cycle Wiki diagram and elevation of nuclear-targeted *PPARGC1A* (Figure 6B).

String_db. String database functional analysis was also conducted on subclone datasets, where the *LDHA/B* DKO *versus* WT down-regulated DEGs involved losses in oxidoreductase activities, aldehyde dehydrogenase activities, anion transporter activity, and corresponding increases in transcripts associated with proteins involved with response/defense to viral and other organisms, hexose/fructose metabolism and RIG-I-like receptor signaling (Figure 7A, B). Notably, there was a large integrated response evoked by dual knock down in *LDHA/B* DKO as elucidated by this analysis; the reason for this remains unknown. String database functional analysis on the *GPI* KO *versus* WT transcriptome was conducted in both directions, where down-regulated DEGs involved losses in drug detoxification processes, some specific to doxorubicin/daunorubicin, carboxylic acid metabolic systems, oxidoreductase activity and gluconeogenesis, corresponding to a rise in cell response to hypoxia, HIF1 signaling, oxidation-reduction processes, dioxygenase activity, and hexose metabolic processing (Figure 7C, D).

Discussion

Energy reprogramming. The data in this study provide evidence to suggest that severe compromise to glycolysis in colon adenocarcinoma LS174T cells can be achieved by selective dual KO of *LDHA/B* or single KO of the *glucose-6-phosphate isomerase* (*GPI*) gene, and is of little consequence to overall cell survival. Both KO clones display suppression of lactic acid secretion, either inability or strong reduction in glucose consumption, high production of ATP, greater mitochondrial functions and a slower proliferative growth rate (data not shown), as previously reported (17, 18).

Table I. *WT affymetrix human transcriptome: WT versus LDHA/B DKO LS174T colon adenocarcinoma cells.*

Control WT Avg (log2)	LDHA/B DKO Avg (log2)	Fold change	*p*-Value	FDR *p*-Value	Gene symbol	Description
8.3	4.3	–15.5	2.8×10^{-12}	1.0×10^{-8}	MUC6	Mucin 6, oligomeric mucus/gel-forming
8.4	5.0	–11.0	7.5×10^{-8}	3.5×10^{-5}	DKK4	Dickkopf WNT signaling pathway inhibitor 4
6.4	3.0	–10.6	2.2×10^{-13}	4.7×10^{-9}	ANPEP	Alanyl (membrane) aminopeptidase
6.7	3.8	–7.7	4.4×10^{-13}	4.7×10^{-9}	EPS8L3	EPS8-like 3
7.0	4.1	–7.4	1.2×10^{-12}	7.1×10^{-9}	SLC44A4	Solute carrier family 44, member 4
7.6	4.7	–7.3	1.0×10^{-4}	1.2×10^{-2}	BGN	Biglycan
7.5	4.8	–6.3	1.3×10^{-11}	3.4×10^{-8}	LDHB	Lactate dehydrogenase B
6.2	3.6	–6.3	2.5×10^{-11}	5.4×10^{-8}	CPNE2	Copine II
5.7	3.2	–5.7	1.7×10^{-12}	9.0×10^{-9}	DSC3	Desmocollin 3
5.7	3.2	–5.6	8.2×10^{-7}	2.0×10^{-4}	CRYBB1	Crystallin beta B1
5.8	3.3	–5.4	1.2×10^{-9}	1.4×10^{-6}	AKR1C2	Aldo-keto reductase family 1, member C2
7.6	5.4	–4.7	1.9×10^{-13}	4.7×10^{-9}	AKR1B10	Aldo-keto reductase family 1, member B10
5.3	3.1	–4.5	9.9×10^{-6}	1.6×10^{-3}	LINC00942	Long intergenic non-protein coding RNA 942
6.5	4.5	–4.1	5.6×10^{-11}	1.1×10^{-7}	SLC9A2	Solute carrier family 9, subfamily A
6.6	4.6	–4.0	4.4×10^{-9}	4.1×10^{-6}	LDHA	Lactate dehydrogenase A
6.0	4.0	–4.0	1.1×10^{-7}	4.6×10^{-5}	GAL	Galanin/GMAP prepropeptide
5.6	3.6	–3.9	5.0×10^{-11}	1.0×10^{-7}	WWC2	WW and C2 domain containing 2
8.2	6.2	–3.9	1.2×10^{-2}	1.8×10^{-1}	CYP1A2	Cytochrome P450, family 1, sf A, polypeptide 2
5.2	3.2	–3.8	1.7×10^{-6}	4.0×10^{-4}	HULC	H.C up-regulated long non-coding RNA
6.3	4.3	–3.8	6.3×10^{-10}	8.2×10^{-7}	ABCC2	ATP binding cassette subfamily C member 2
7.9	6.1	–3.5	2.9×10^{-12}	1.0×10^{-8}	MSN	Moesin
5.1	3.3	–3.5	2.8×10^{-10}	4.3×10^{-7}	BCL11A	B-cell CLL/lymphoma 11A (zinc finger protein)
4.5	2.7	–3.4	6.0×10^{-5}	6.1×10^{-3}	NOX1	NADPH oxidase 1
4.9	3.1	–3.4	3.5×10^{-6}	7.0×10^{-4}	HUNK	Hormonally up-regulated Neu-associated kinase
6.8	5.1	–3.4	2.4×10^{-2}	2.6×10^{-1}	CHAC1	ChaC glutathionx10-specific gamma-glutamylcyclotransferase 1
5.7	4.0	–3.3	7.0×10^{-9}	5.7×10^{-6}	THSD4	Thrombospondin type 1 domain containing 4
7.3	5.6	–3.3	2.1×10^{-9}	2.2×10^{-6}	CDH3	Cadherin 3, type 1, P-cadherin (placental)
7.2	5.5	–3.2	3.7×10^{-7}	1.0×10^{-4}	ETV4	Ets variant 4
5.3	3.6	–3.2	1.4×10^{-5}	2.0×10^{-3}	HBE1	Hemoglobin, epsilon 1
5.5	3.8	–3.2	9.1×10^{-9}	7.0×10^{-6}	CLIC3	Chloride intracellular channel 3
5.2	3.6	–3.1	2.9×10^{-7}	1.0×10^{-4}	IGFBP2	Insulin like growth factor binding protein 2
7.1	5.4	–3.1	2.9×10^{-5}	3.6×10^{-3}	CALB2	Calbindin 2
8.3	6.7	–3.0	3.7×10^{-6}	8.0×10^{-4}	ALDH3A1	Aldehyde dehydrogenase 3 family, member A1
5.4	3.8	–3.0	5.8×10^{-7}	2.0×10^{-4}	CAMK2N1	Calcium/calmodulin-dependent protein kinase II inhibitor 1
6.2	4.6	–2.9	6.1×10^{-9}	5.2×10^{-6}	PTPN18	Protein tyrosine phosphatase, non-receptor type 18 (brain-derived)
4.3	2.8	–2.9	1.7×10^{-8}	1.1×10^{-5}	EDARADD	EDAR-associated death domain
6.1	4.6	–2.9	5.4×10^{-7}	2.0×10^{-4}	FGFBP1	Fibroblast growth factor binding protein 1
4.1	2.7	–2.8	6.7×10^{-8}	3.2×10^{-5}	SPIN3	Spindlin family, member 3
5.6	4.2	–2.8	4.8×10^{-6}	9.0×10^{-4}	CORO2A	Coronin, actin binding protein, 2A
4.1	2.7	–2.7	7.0×10^{-4}	3.4×10^{-2}	OR51B4	Olfactory receptor, family 51, subfamily B, member 4
5.8	4.4	–2.7	6.0×10^{-4}	2.9×10^{-2}	EIF2B5-AS1	EIF2B5 antisense RNA 1
8.2	6.7	–2.7	1.5×10^{-5}	2.2×10^{-3}	GPX2	Glutathione peroxidase 2
2.9	1.5	–2.7	6.3×10^{-7}	2.0×10^{-4}	GPX8	Glutathione peroxidase 8 (putative)
4.7	3.2	–2.7	5.3×10^{-9}	4.6×10^{-6}	ANOS1	Anosmin 1
10.3	8.9	–2.7	8.5×10^{-6}	1.4×10^{-3}	SLC7A11	Solute carrier family 7 (anionic amino acid transporter light chain, xc- system), member 11
6.3	4.8	–2.7	9.7×10^{-3}	1.6×10^{-1}	VCAN	Versican
5.9	4.5	–2.7	1.5×10^{-6}	4.0×10^{-4}	SLPI	Secretory leukocyte peptidase inhibitor
6.1	4.7	–2.7	2.6×10^{-9}	2.7×10^{-6}	TFCP2	Transcription factor CP2
5.8	4.4	–2.7	8.0×10^{-8}	3.7×10^{-5}	DNM1	Dynamin 1
5.0	3.5	–2.6	9.3×10^{-3}	1.6×10^{-1}	IL37	Interleukin 37
4.8	3.4	–2.6	3.4×10^{-8}	1.9×10^{-5}	ANO1	Anoctamin 1, calcium activated chloride channel
7.2	5.8	–2.6	4.6×10^{-11}	9.7×10^{-8}	CA12	Carbonic anhydrase XII
5.8	4.4	–2.6	5.5×10^{-6}	1.0×10^{-3}	CES1; CES1P1	Carboxylesterase 1; carboxylesterase 1 pseudogene 1
4.2	2.8	–2.6	1.1×10^{-8}	7.8×10^{-6}	ALDH1A1	Aldehyde dehydrogenase 1 family, member A1
4.2	2.8	–2.6	1.8×10^{-8}	1.2×10^{-5}	LYZ	Lysozyme

Table I. *Continued*

Table I. *Continued*

Control WT Avg (log2)	LDHA/B DKO Avg (log2)	Fold change	*p*-Value	FDR *p*-Value	Gene symbol	Description
6.3	4.9	–2.5	4.6×10^{-9}	4.1×10^{-6}	LCN2	Lipocalin 2
4.9	3.6	–2.5	2.3×10^{-8}	1.5×10^{-5}	TCEA3	Transcription elongation factor A (SII), 3
4.7	3.3	–2.5	1.6×10^{-8}	1.1×10^{-5}	GREB1L	Growth regulation by estrogen in breast cancer-like
7.9	6.6	–2.5	3.4×10^{-9}	3.4×10^{-6}	CLDN3	Claudin 3
4.6	3.3	–2.5	8.4×10^{-6}	1.4×10^{-3}	TET1	Tet methylcytosine dioxygenase 1
6.8	5.6	–2.5	4.7×10^{-3}	1.1×10^{-1}	LCN15	Lipocalin 15
5.3	4.0	–2.5	3.2×10^{-6}	7.0×10^{-4}	SOD3	Superoxide dismutase 3, extracellular
4.9	3.6	–2.4	1.2×10^{-9}	1.4×10^{-6}	FXYD5	FXYD domain containing ion transport regulator 5
7.1	5.9	–2.4	2.5×10^{-8}	1.5×10^{-5}	SLC44A2	Solute carrier family 44 (choline transporter), member 2
3.5	2.3	–2.4	3.9×10^{-8}	2.1×10^{-5}	TSPAN7	Tetraspanin 7
3.7	2.4	–2.4	6.0×10^{-4}	3.2×10^{-2}	TREX2	Three prime repair exonuclease 2
6.0	4.7	–2.3	3.6×10^{-9}	3.5×10^{-6}	FGF19	Fibroblast growth factor 19
3.8	2.6	–2.3	1.3×10^{-5}	1.9×10^{-3}	SRGAP1	SLIT-ROBO Rho GTPase activating protein 1
3.9	2.7	–2.3	9.8×10^{-5}	8.8×10^{-3}	ALDH2	Aldehyde dehydrogenase 2 family (mitochondrial)
5.4	4.2	–2.3	3.9×10^{-6}	8.0×10^{-4}	GCNT3	Glucosaminyl (N-acetyl) transferase 3, mucin type
6.2	5.0	–2.3	1.3×10^{-7}	5.4×10^{-5}	PFKP	Phosphofructokinase, platelet
3.9	2.7	–2.3	1.8×10^{-5}	2.5×10^{-3}	IL1A	Interleukin 1 alpha
6.8	5.6	–2.3	3.5×10^{-2}	3.1×10^{-1}	CTH	Cystathionine gamma-lyase
6.8	5.6	–2.3	2.6×10^{-6}	6.0×10^{-4}	RCN1	Reticulocalbin 1, EF-hand calcium binding domain
9.4	8.2	–2.3	4.1×10^{-5}	4.7×10^{-3}	ASS1	Argininosuccinate synthase 1
5.1	4.0	–2.2	3.3×10^{-5}	3.9×10^{-3}	SYNE4	Spectrin repeat containing, nuclear envelope family member 4
4.2	3.1	–2.2	6.3×10^{-8}	3.1×10^{-5}	TRIM7	Tripartite motif containing 7
6.0	4.9	–2.2	2.6×10^{-7}	9.2×10^{-5}	PAH	Phenylalanine hydroxylase
5.0	3.8	–2.2	6.3×10^{-6}	1.1×10^{-3}	SLC16A5	Solute carrier family 16 (monocarboxylate transporter), member 5
5.1	4.0	–2.2	6.7×10^{-7}	2.0×10^{-4}	LAMB2	Laminin, beta 2 (laminin S)
5.0	3.9	–2.2	5.0×10^{-4}	2.6×10^{-2}	ATP9A	ATPase, class II, type 9A
5.4	4.3	–2.2	1.4×10^{-5}	2.0×10^{-3}	ABAT	4-aminobutyrate aminotransferase
6.5	5.4	–2.2	1.6×10^{-2}	2.1×10^{-1}	ATP2C2	ATPase, Ca++ transporting, type 2C, member 2
5.6	4.5	–2.2	9.8×10^{-8}	4.3×10^{-5}	EFNA3	Ephrin-A3
5.9	4.8	–2.2	1.0×10^{-4}	9.6×10^{-3}	CORO1A	Coronin, actin binding protein, 1A
5.9	4.8	–2.2	7.0×10^{-9}	5.7×10^{-6}	PLA2G16	Phospholipase A2, group XVI
4.5	3.4	–2.2	4.4×10^{-5}	4.9×10^{-3}	PTPRU	Protein tyrosine phosphatase, receptor type, U
4.0	2.9	–2.2	3.8×10^{-7}	1.0×10^{-4}	SPATA6L	Spermatogenesis associated 6-like
5.1	4.0	–2.1	2.0×10^{-4}	1.3×10^{-2}	SNORA11; MAGED2	Small nucleolar RNA, H/ACA box 11; MAGE family member D2
5.0	3.9	–2.1	6.4×10^{-6}	1.1×10^{-3}	AKR1C1	Aldo-keto reductase family 1, member C1
6.3	5.2	–2.1	2.3×10^{-7}	8.6×10^{-5}	FUOM	Fucose mutarotase
5.2	4.2	–2.1	2.4×10^{-9}	2.5×10^{-6}	CYP2J2	Cytochrome P450, family 2, subfamily J, polypeptide 2
5.2	4.1	–2.1	6.1×10^{-5}	6.2×10^{-3}	CAPN5	Calpain 5
7.3	6.2	–2.1	5.2×10^{-6}	1.0×10^{-3}	HOXB9	Homeobox B9
4.0	2.9	–2.1	9.5×10^{-3}	1.6×10^{-1}	MIR1206	MicroRNA 1206
5.9	4.9	–2.1	4.6×10^{-8}	2.4×10^{-5}	KIZ	Kizuna centrosomal protein
6.3	5.2	–2.1	1.4×10^{-7}	5.7×10^{-5}	SERPINB5	Serpin peptidase inhibitor, clade B (ovalbumin), member 5
5.9	4.8	–2.1	2.7×10^{-2}	2.7×10^{-1}	SLC6A9	Solute carrier family 6 (neurotransmitter transporter, glycine), member 9
6.9	5.9	–2.1	2.1×10^{-2}	2.4×10^{-1}	STC2	Stanniocalcin 2
4.4	3.4	–2.1	4.8×10^{-6}	9.0×10^{-4}	LEMD1; BLACAT1	LEM domain containing 1; bladder cancer associated transcript 1 (non-protein coding)
5.0	4.0	–2.1	1.3×10^{-5}	1.9×10^{-3}	MYH13	Myosin, heavy chain 13, skeletal muscle
4.5	3.5	–2.1	1.5×10^{-6}	4.0×10^{-4}	SLC34A3	Solute carrier family 34 (type II sodium/phosphate cotransporter), member 3
4.4	3.4	–2.1	2.4×10^{-5}	3.1×10^{-3}	AIFM3; LZTR1	Apoptosis-inducing factor, mitochondrion-associated, 3; leucinx10-zipper-like transcription regulator 1
5.2	4.2	–2.1	1.8×10^{-5}	2.5×10^{-3}	CRYBA4	Crystallin beta A4
4.5	3.4	–2.1	4.0×10^{-4}	2.3×10^{-2}	INAFM2	InaF-motif containing 2

Table I. *Continued*

Table I. *Continued*

Control WT Avg (log2)	LDHA/B DKO Avg (log2)	Fold change	*p*-Value	FDR *p*-Value	Gene symbol	Description
2.9	1.8	–2.1	1.7×10^{-6}	4.0×10^{-4}	OR51B5; HBG2; HBE1	Olfactory receptor, family 51, subfamily B, member 5; hemoglobin, gamma G; hemoglobin, epsilon 1
5.6	4.6	–2.1	8.2×10^{-8}	3.8×10^{-5}	DMTN	Dematin actin binding protein
6.9	5.9	–2.1	3.7×10^{-8}	2.0×10^{-5}	PLLP	Plasmolipin
3.4	2.3	–2.1	2.1×10^{-6}	5.0×10^{-4}	GXYLT2	Glucoside xylosyltransferase 2
6.2	5.2	–2.0	9.7×10^{-5}	8.7×10^{-3}	LIF	Leukemia inhibitory factor
2.5	1.5	–2.0	8.0×10^{-3}	1.5×10^{-1}	MIR3646	MicroRNA 3646
7.2	6.2	–2.0	2.0×10^{-9}	2.2×10^{-6}	TMEM214	Transmembrane protein 214
5.1	4.0	–2.0	1.9×10^{-8}	1.2×10^{-5}	TPST2	Tyrosylprotein sulfotransferase 2
6.2	5.2	–2.0	7.3×10^{-6}	1.3×10^{-3}	APCDD1	Adenomatosis polyposis coli down-regulated 1
6.4	5.4	–2.0	1.0×10^{-4}	9.2×10^{-3}	COTL1	Coactosin-like F-actin binding protein 1
3.1	4.1	2.0	6.8×10^{-5}	6.8×10^{-3}	CXCL10	Chemokine (C-X-C motif) ligand 10
3.3	4.3	2.0	1.6×10^{-2}	2.1×10^{-1}	SCARNA15; SNHG21	Small Cajal body-specific RNA 15; small nucleolar RNA host gene 21
8.1	9.1	2.0	4.4×10^{-8}	2.3×10^{-5}	TXNIP	Thioredoxin interacting protein
3.4	4.4	2.0	6.0×10^{-4}	3.1×10^{-2}	TOX3	TOX high mobility group box family member 3
3.7	4.7	2.0	9.3×10^{-6}	1.5×10^{-3}	C2orf54	Chromosome 2 open reading frame 54
6.0	7.0	2.0	1.4×10^{-8}	1.0×10^{-5}	ISG15	ISG15 ubiquitin-like modifier
3.9	4.9	2.0	1.6×10^{-6}	4.0×10^{-4}	FAM230B	Family with sequence similarity 230, member B (non-protein coding)
3.7	4.7	2.0	4.0×10^{-4}	2.2×10^{-2}	IFI16	Interferon, gamma-inducible protein 16
2.9	3.9	2.0	2.6×10^{-3}	7.8×10^{-2}	LYST	Lysosomal trafficking regulator
4.4	5.4	2.1	3.9×10^{-5}	4.5×10^{-3}	IFIH1	Interferon induced, with helicase C domain 1
3.7	4.7	2.1	1.1×10^{-2}	1.7×10^{-1}	RNU1-13P	RNA, U1 small nuclear 13, pseudogene
3.7	4.7	2.1	1.1×10^{-2}	1.7×10^{-1}	RNU1-13P	RNA, U1 small nuclear 13, pseudogene
6.2	7.3	2.1	3.0×10^{-6}	6.0×10^{-4}	ARRDC4	Arrestin domain containing 4
4.1	5.1	2.1	2.5×10^{-8}	1.5×10^{-5}	CHST15	Carbohydrate (N-acetylgalactosamine 4-sulfate 6-O) sulfotransferase 15
3.6	4.7	2.1	1.1×10^{-2}	1.8×10^{-1}	AGR3	Anterior gradient 3, protein disulphide isomerase family member
3.3	4.3	2.1	7.3×10^{-3}	1.4×10^{-1}	MIR3620; ARF1	MicroRNA 3620; ADP-ribosylation factor 1
3.2	4.2	2.1	2.2×10^{-5}	2.9×10^{-3}	MIR3622A	MicroRNA 3622a
6.4	7.5	2.1	3.0×10^{-4}	1.9×10^{-2}	SCARNA4	Small Cajal body-specific RNA 4
4.6	5.7	2.2	5.2×10^{-5}	5.6×10^{-3}	OASL	2-5-oligoadenylate synthetasx10-like
1.9	3.0	2.2	7.0×10^{-4}	3.5×10^{-2}	MIR4727	MicroRNA 4727
5.7	6.8	2.2	1.8×10^{-5}	2.5×10^{-3}	SECTM1	Secreted and transmembrane 1
4.5	5.7	2.2	4.5×10^{-9}	4.1×10^{-6}	SATB1	SATB homeobox 1
4.4	5.5	2.2	1.3×10^{-2}	1.9×10^{-1}	SCARNA3	Small Cajal body-specific RNA 3
6.4	7.6	2.2	2.0×10^{-4}	1.2×10^{-2}	XAF1	XIAP associated factor 1
3.6	4.8	2.3	7.4×10^{-3}	1.4×10^{-1}	ARMC3	Armadillo repeat containing 3
5.9	7.1	2.3	1.4×10^{-5}	2.1×10^{-3}	LYST	Lysosomal trafficking regulator
2.9	4.1	2.3	3.0×10^{-4}	2.0×10^{-2}	C6orf222	Chromosome 6 open reading frame 222
7.9	9.2	2.4	9.0×10^{-8}	4.1×10^{-5}	GPR137B	G protein-coupled receptor 137B
4.0	5.3	2.4	6.4×10^{-7}	2.0×10^{-4}	DUSP10	Dual specificity phosphatase 10
3.1	4.3	2.4	8.9×10^{-5}	8.2×10^{-3}	LDB2	LIM domain binding 2
8.5	9.8	2.4	1.0×10^{-2}	1.7×10^{-1}	SNORA23	Small nucleolar RNA, H/ACA box 23
6.7	8.0	2.4	5.4×10^{-6}	1.0×10^{-3}	HMGCS2	3-hydroxy-3-methylglutaryl-CoA synthase 2 (mitochondrial)
5.3	6.6	2.4	9.5×10^{-6}	1.5×10^{-3}	PLSCR1	Phospholipid scramblase 1
6.4	7.7	2.5	2.3×10^{-7}	8.6×10^{-5}	HERC6	HECT and RLD domain containing E3 ubiquitin protein ligase family member 6
3.6	4.9	2.5	1.7×10^{-8}	1.1×10^{-5}	ALOX12P2	Arachidonate 12-lipoxygenase pseudogene 2
1.1	2.5	2.5	2.5×10^{-2}	2.6×10^{-1}	MIR642B	MicroRNA 642b
2.1	3.4	2.5	1.7×10^{-3}	5.9×10^{-2}	KRTAP10-1	Keratin associated protein 10-1
1.6	3.0	2.5	1.1×10^{-5}	1.7×10^{-3}	OR51C1P	Olfactory receptor, family 51, subfamily C, member 1 pseudogene
5.5	6.8	2.5	1.0×10^{-6}	3.0×10^{-4}	IFI27	Interferon, alpha-inducible protein 27

Table I. *Continued*

Table I. *Continued*

Control WT Avg (log2)	LDHA/B DKO Avg (log2)	Fold change	*p*-Value	FDR *p*-Value	Gene symbol	Description
3.3	4.6	2.5	3.6×10^{-8}	2.0×10^{-5}	ZSCAN12P1	Zinc finger and SCAN domain containing 12 pseudogene 1
2.1	3.5	2.6	3.0×10^{-8}	1.7×10^{-5}	UBE2U	Ubiquitin-conjugating enzyme E2U (putative)
5.1	6.4	2.6	5.2×10^{-10}	7.2×10^{-7}	SEMA6A	Sema domain, transmembrane domain (TM), and cytoplasmic domain, (semaphorin) 6A
8.0	9.4	2.6	7.0×10^{-11}	1.3×10^{-7}	SMOC2	SPARC related modular calcium binding 2
5.1	6.5	2.7	3.8×10^{-8}	2.1×10^{-5}	SAMD9	Sterile alpha motif domain containing 9
6.5	7.9	2.7	1.1×10^{-7}	4.7×10^{-5}	SNORA75	Small nucleolar RNA, H/ACA box 75
4.0	5.4	2.7	7.6×10^{-6}	1.3×10^{-3}	NR0B2	Nuclear receptor subfamily 0, group B, member 2
2.5	3.9	2.7	2.6×10^{-8}	1.5×10^{-5}	LOC101927859; LOC105369185; LOC105372941	Serine/arginine repetitive matrix protein 2-like; uncharacterized LOC105369185; uncharacterized LOC105372941
5.1	6.5	2.7	4.0×10^{-4}	2.5×10^{-2}	PCK1	Phosphoenolpyruvate carboxykinase 1 (soluble)
3.5	5.0	2.7	3.3×10^{-7}	1.0×10^{-4}	NPC1L1	NPC1-like 1
2.8	4.3	2.8	1.0×10^{-2}	1.7×10^{-1}	MIR4659A	MicroRNA 4659a
4.3	5.8	2.8	6.2×10^{-9}	5.3×10^{-6}	SAMD9L	Sterile alpha motif domain containing 9-like
4.8	6.4	2.9	1.9×10^{-5}	2.5×10^{-3}	LINC00520	Long intergenic non-protein coding RNA 520
2.8	4.3	2.9	1.6×10^{-10}	2.8×10^{-7}	CSF2RA	Colony stimulating factor 2 receptor, alpha, low-affinity (granulocytx10-macrophage)
3.0	4.6	3.0	8.4×10^{-9}	6.5×10^{-6}	ASB4	Ankyrin repeat and SOCS box containing 4
5.2	6.8	3.0	1.7×10^{-8}	1.1×10^{-5}	ENC1	Ectodermal-neural cortex 1 (with BTB domain)
2.8	4.4	3.2	4.2×10^{-2}	3.4×10^{-1}	SNORA2A	Small nucleolar RNA, H/ACA box 2A
5.6	7.3	3.2	3.5×10^{-7}	1.0×10^{-4}	DDX58	DEAD (Asp-Glu-Ala-Asp) box polypeptide 58
2.5	4.2	3.2	2.3×10^{-8}	1.5×10^{-5}	TUSC3	Tumor suppressor candidate 3
6.7	8.4	3.3	9.2×10^{-8}	4.2×10^{-5}	CD68	CD68 molecule
4.3	6.0	3.4	6.7×10^{-10}	8.5×10^{-7}	PADI1	Peptidyl arginine deiminase, type I
3.9	5.7	3.4	3.8×10^{-10}	5.4×10^{-7}	PPARGC1A	Peroxisome proliferator-activated receptor gamma, coactivator 1 alpha
4.8	6.7	3.7	3.0×10^{-10}	4.6×10^{-7}	IFIT1	Interferon-induced protein with tetratricopeptide repeats 1
3.6	5.5	3.8	3.4×10^{-7}	1.0×10^{-4}	IFIT3	Interferon-induced protein with tetratricopeptide repeats 3
2.5	4.4	3.9	7.6×10^{-7}	2.0×10^{-4}	PRDM9	PR domain containing 9
4.4	6.5	4.2	2.4×10^{-7}	8.8×10^{-5}	RSAD2	Radical S-adenosyl methionine domain containing 2
4.9	7.0	4.3	1.5×10^{-8}	1.1×10^{-5}	IRF9	Interferon regulatory factor 9
5.6	7.7	4.3	4.5×10^{-8}	2.3×10^{-5}	IGFBP7	Insulin like growth factor binding protein 7
5.2	7.4	4.4	6.1×10^{-6}	1.1×10^{-3}	DDX60	DEAD (Asp-Glu-Ala-Asp) box polypeptide 60
4.8	7.0	4.4	4.8×10^{-12}	1.5×10^{-8}	DEFB1	Defensin, beta 1
3.4	5.6	4.6	4.9×10^{-13}	4.7×10^{-9}	NEO1	Neogenin 1
8.2	10.4	4.7	2.6×10^{-8}	1.5×10^{-5}	IFI6	Interferon, alpha-inducible protein 6
4.9	7.2	4.7	1.3×10^{-10}	2.3×10^{-7}	FXYD4	FXYD domain containing ion transport regulator 4
5.1	7.3	4.9	1.6×10^{-7}	6.2×10^{-5}	IFI44	Interferon-induced protein 44
2.6	5.0	5.1	8.8×10^{-8}	4.1×10^{-5}	IFI44L	Interferon-induced protein 44-like
4.7	7.2	5.6	2.0×10^{-4}	1.3×10^{-2}	SPINK1	Serine peptidase inhibitor, Kazal type 1
1.9	4.4	5.8	9.8×10^{-8}	4.3×10^{-5}	NTS	Neurotensin
4.2	6.8	6.0	2.2×10^{-11}	5.0×10^{-8}	OAS2	2-5-oligoadenylate synthetase 2
2.8	5.8	7.7	2.1×10^{-9}	2.2×10^{-6}	CFAP126	Cilia and flagella associated protein 126

Typically, malignant tumor cells respond to high concentrations of glucose or insulin (fed state) by induction of gene transcripts and activation of mTOR signaling to augment glucose transporters, glycolytic enzymes, and enable higher production of succinyl-CoA and malonyl-CoA metabolites, which inhibit fatty acid oxidation as an alternative fuel source, coinciding with the *Warburg effect*. In this study we show that glycolysis-null KO clones undergo a transcriptomic shift consistent with glucose deprivation signaling (response to long term fasting), with increased transcription of mitochondrial *HMGCS2* (HMG-CoA synthetase) and *PPARγ coactivator-1α* (*PGC-1α*), both associated with loss of mTOR signaling (24). The high expression of *PGC-1α* reported leads to heightened AMPK phospho-signaling, which normally plays a role in long-chain fatty acid catabolism, inactivation of acetyl-CoA carboxylase

Table II. *WT affymetrix human transcriptome: WT versus GPI KO LS174T colon adenocarcinoma cells.*

GPI KO Avg (log2)	Ctrl Avg (log2)	Fold change	*p*-Value	FDR *p*-Value	Gene symbol	Description
4.0	8.4	–20.6	2.1×10^{-8}	2.0×10^{-5}	DKK4	Dickkopf WNT signaling pathway inhibitor 4
2.4	6.3	–14.8	1.1×10^{-14}	1.7×10^{-10}	GJA1	Gap junction protein alpha 1
2.8	6.3	–10.7	1.3×10^{-5}	2.8×10^{-3}	VCAN	Versican
4.5	7.6	–8.4	3.0×10^{-4}	2.2×10^{-2}	BGN	Biglycan
4.1	7.1	–7.8	1.4×10^{-6}	5.0×10^{-4}	CALB2	Calbindin 2
2.8	5.8	–7.6	2.5×10^{-10}	5.5×10^{-7}	AKR1C2	Aldo-keto reductase family 1, member C2
3.0	5.8	–7.1	6.7×10^{-14}	6.5×10^{-10}	ZNF607	Zinc finger protein 607
2.8	5.5	–6.5	4.1×10^{-13}	3.3×10^{-9}	SP8	Sp8 transcription factor
3.1	5.7	–5.9	1.0×10^{-11}	5.3×10^{-8}	DSC3	Desmocollin 3
7.3	9.8	–5.8	8.1×10^{-15}	1.7×10^{-10}	GPI	Glucose 6-phosphate isomerase
3.7	6.2	–5.7	1.7×10^{-10}	4.3×10^{-7}	APCDD1	Adenomatosis polyposis coli down-regulated 1
5.0	7.3	–4.7	5.0×10^{-11}	1.7×10^{-7}	HOXB9	Homeobox B9
4.1	6.3	–4.7	6.5×10^{-8}	5.2×10^{-5}	TIMP1	TIMP metallopeptidase inhibitor 1
2.9	5.2	–4.7	4.5×10^{-8}	4.0×10^{-5}	PCDHB13	Protocadherin beta 13
5.1	7.3	–4.7	1.1×10^{-11}	5.3×10^{-8}	CCND2	Cyclin D2
6.0	8.2	–4.5	1.8×10^{-6}	6.0×10^{-4}	GPX2	Glutathione peroxidase 2
4.5	6.6	–4.4	1.4×10^{-12}	9.5×10^{-9}	HOXB6; HOXB3	Homeobox B6; homeobox B3
2.8	4.9	–4.2	6.3×10^{-7}	3.0×10^{-4}	HUNK	Hormonally up-regulated Neu-associated kinase
3.2	5.2	–3.9	5.6×10^{-6}	1.5×10^{-3}	HULC	Hepatocellular carcinoma up-regulated long non-coding RNA
3.9	5.8	–3.9	1.3×10^{-5}	2.9×10^{-3}	EIF2B5-AS1	EIF2B5 antisense RNA 1
3.9	5.7	–3.7	6.4×10^{-10}	1.3×10^{-6}	HOXB5	Homeobox B5
6.4	8.3	–3.6	7.4×10^{-6}	1.8×10^{-3}	ALDH3A1	Aldehyde dehydrogenase 3 family, member A1
5.8	7.6	–3.4	5.0×10^{-4}	2.8×10^{-2}	ANXA1	Annexin A1
5.8	7.6	–3.4	1.3×10^{-10}	3.7×10^{-7}	AKR1B10	Aldo-keto reductase family 1, member B10 (aldose reductase)
2.8	4.5	–3.3	6.2×10^{-6}	1.6×10^{-3}	MIR196A1	MicroRNA 196a-1
3.6	5.3	–3.2	5.0×10^{-6}	1.4×10^{-3}	HBE1	Hemoglobin, epsilon 1
4.8	6.5	–3.2	5.1×10^{-6}	1.4×10^{-3}	KLK7	Kallikrein related peptidase 7
4.1	5.7	–3.1	2.0×10^{-4}	1.5×10^{-2}	CRYBB1	Crystallin beta B1
3.7	5.3	–3.1	6.2×10^{-8}	5.1×10^{-5}	SKAP1	Src kinase associated phosphoprotein 1
2.5	4.1	–3.1	5.0×10^{-4}	3.0×10^{-2}	OR51B4	Olfactory receptor, family 51, subfamily B, member 4
1.8	3.4	–3.1	4.0×10^{-4}	2.6×10^{-2}	MIR548X	MicroRNA 548x
3.1	4.7	–3.0	2.0×10^{-4}	1.8×10^{-2}	TM4SF4	Transmembrane 4 L six family member 4
4.4	5.9	–3.0	3.3×10^{-5}	5.4×10^{-3}	ANKRD22	Ankyrin repeat domain 22
4.2	5.7	–2.9	2.3×10^{-9}	3.8×10^{-6}	MFSD2A	Major facilitator superfamily domain containing 2A
4.2	5.7	–2.9	1.3×10^{-7}	8.8×10^{-5}	THSD4	Thrombospondin type 1 domain containing 4
2.7	4.2	–2.8	2.0×10^{-8}	2.0×10^{-5}	ALDH1A1	Aldehyde dehydrogenase 1 family, member A1
6.0	7.5	–2.8	8.8×10^{-10}	1.6×10^{-6}	PLA2G4A	Phospholipase A2, group IVA (cytosolic, calcium-dependent)
4.4	5.8	–2.7	1.5×10^{-9}	2.5×10^{-6}	FAM171B	Family with sequence similarity 171, member B
8.0	9.3	–2.6	1.1×10^{-5}	2.4×10^{-3}	DPEP1	Dipeptidase 1 (renal)
6.1	7.5	–2.6	1.5×10^{-8}	1.6×10^{-5}	ID1	Inhibitor of DNA binding 1, dominant negative helix-loop-helix protein
3.3	4.7	–2.6	2.1×10^{-8}	2.0×10^{-5}	ANOS1	Anosmin 1
3.9	5.3	–2.6	2.3×10^{-5}	4.2×10^{-3}	FAR2P1	Fatty acyl-CoA reductase 2 pseudogene 1
4.7	6.1	–2.6	6.8×10^{-6}	1.7×10^{-3}	SLC6A20	Solute carrier family 6 (proline IMINO transporter), member 20
1.6	2.9	–2.5	3.1×10^{-6}	1.0×10^{-3}	GPX8	Glutathione peroxidase 8 (putative)
3.7	5.0	–2.5	6.6×10^{-7}	3.0×10^{-4}	AKR1C1	Aldo-keto reductase family 1, member C1
2.7	4.0	–2.5	2.0×10^{-7}	1.0×10^{-4}	MECOM	MDS1 and EVI1 complex locus
4.6	5.9	–2.5	3.0×10^{-9}	4.5×10^{-6}	PLA2G16	Phospholipase A2, group XVI
5.3	6.6	–2.5	8.4×10^{-6}	2.0×10^{-3}	AREG	Amphiregulin
5.1	6.4	–2.5	1.8×10^{-6}	6.0×10^{-4}	AKR1C3	Aldo-keto reductase family 1, member C3
3.0	4.3	–2.4	7.6×10^{-8}	5.9×10^{-5}	CCND2-AS1	CCND2 antisense RNA 1
2.3	3.6	–2.4	2.4×10^{-3}	7.2×10^{-2}	ANKRD36BP1	Ankyrin repeat domain 36B pseudogene 1
5.8	7.0	–2.4	1.3×10^{-5}	2.8×10^{-3}	AREG	Amphiregulin
9.0	10.3	–2.4	1.0×10^{-4}	1.4×10^{-2}	ND6	NADH dehydrogenase, subunit 6 (complex I)

Table II. *Continued*

Table II. *Continued*

GPI KO Avg (log2)	Ctrl Avg (log2)	Fold change	*p*-Value	FDR *p*-Value	Gene symbol	Description
1.7	2.9	–2.4	1.0×10^{-4}	1.4×10^{-2}	GATSL2	GATS protein-like 2
3.3	4.5	–2.4	4.1×10^{-5}	6.2×10^{-3}	IGFL4	IGF like family member 4
2.9	4.1	–2.3	9.2×10^{-8}	6.8×10^{-5}	HOXB3	Homeobox B3
5.8	7.0	–2.3	3.0×10^{-5}	5.0×10^{-3}	ADIRF	Adipogenesis regulatory factor
6.2	7.4	–2.3	8.2×10^{-11}	2.5×10^{-7}	SEC31A	SEC31 homolog A, COPII coat complex component
5.0	6.2	–2.3	1.7×10^{-8}	1.7×10^{-5}	HOXB7	Homeobox B7
2.5	3.7	–2.3	8.2×10^{-7}	4.0×10^{-4}	BCHE	Butyrylcholinesterase
7.1	8.3	–2.3	1.3×10^{-2}	1.7×10^{-1}	MUC6	Mucin 6, oligomeric mucus/gel-forming
3.9	5.1	–2.3	2.5×10^{-6}	8.0×10^{-4}	BCL11A	B-cell CLL/lymphoma 11A (zinc finger protein)
5.7	6.9	–2.3	3.1×10^{-2}	2.6×10^{-1}	ROCK1P1	Rho-associated, coiled-coil containing protein kinase 1 pseudogene 1
9.1	10.3	–2.3	7.5×10^{-5}	9.2×10^{-3}	SLC7A11	Solute carrier family 7 (anionic amino acid transporter light chain, xc- system), member 11
3.4	4.5	–2.2	1.9×10^{-8}	1.9×10^{-5}	SATB1	SATB homeobox 1
4.9	6.1	–2.2	1.2×10^{-7}	8.2×10^{-5}	IFITM2	Interferon induced transmembrane protein 2
4.4	5.6	–2.2	1.1×10^{-6}	5.0×10^{-4}	SIPA1L2	Signal-induced proliferation-associated 1 like 2
2.2	3.4	–2.2	2.7×10^{-6}	9.0×10^{-4}	GXYLT2	Glucoside xylosyltransferase 2
4.8	5.9	–2.2	1.7×10^{-3}	6.1×10^{-2}	UCA1	Urothelial cancer associated 1 (non-protein coding)
8.1	9.2	–2.2	1.4×10^{-2}	1.8×10^{-1}	CTSE	Cathepsin E
3.5	4.6	–2.2	2.8×10^{-5}	4.7×10^{-3}	ZC3H12C	Zinc finger CCCH-type containing 12C
5.4	6.5	–2.2	3.0×10^{-8}	2.8×10^{-5}	ABCC3	ATP binding cassette subfamily C member 3
2.7	3.8	–2.2	4.7×10^{-3}	1.0×10^{-1}	CEP152	Centrosomal protein 152kDa
2.3	3.4	–2.2	4.0×10^{-4}	2.6×10^{-2}	LRRC7	Leucine rich repeat containing 7
1.9	3.0	–2.2	2.4×10^{-3}	7.2×10^{-2}	FAM35DP	Family with sequence similarity 35, member A pseudogene
5.8	6.9	–2.2	7.0×10^{-5}	9.0×10^{-3}	LIPH	Lipase, member H
3.4	4.6	–2.2	9.0×10^{-4}	4.1×10^{-2}	DIP2A-IT1	DIP2A intronic transcript 1
3.4	4.6	–2.2	1.8×10^{-2}	2.0×10^{-1}	DPY19L2P1	DPY19L2 pseudogene 1
2.4	3.5	–2.1	1.9×10^{-2}	2.1×10^{-1}	PIRC66	Piwi-interacting RNA cluster 66
3.8	4.9	–2.1	1.8×10^{-2}	2.0×10^{-1}	HIST1H2AM; HIST1H3J	Histone cluster 1, H2am; histone cluster 1, H3j
3.0	4.0	–2.1	3.0×10^{-5}	5.0×10^{-3}	PAQR8	Progestin and adipoQ receptor family member VIII
5.2	6.3	–2.1	3.0×10^{-4}	2.3×10^{-2}	TM4SF1	Transmembrane 4 L six family member 1
4.9	6.0	–2.1	1.8×10^{-2}	2.0×10^{-1}	GRIN2B	Glutamate receptor, ionotropic, N-methyl D-aspartate 2B
5.0	6.0	–2.1	3.2×10^{-6}	1.0×10^{-3}	CD44	CD44 molecule (Indian blood group)
4.9	5.9	–2.1	3.0×10^{-3}	8.0×10^{-2}	CORO1A	Coronin, actin binding protein, 1A
3.6	4.7	–2.1	2.0×10^{-4}	1.9×10^{-2}	ANKRD20A5P	Ankyrin repeat domain 20 family, member A5, pseudogene
5.1	6.1	–2.1	2.2×10^{-5}	4.0×10^{-3}	FGFBP1	Fibroblast growth factor binding protein 1
2.4	3.5	–2.1	2.9×10^{-2}	2.5×10^{-1}	MIR4497	MicroRNA 4497
2.2	3.3	–2.1	2.7×10^{-5}	4.7×10^{-3}	RAB29	RAB29, member RAS oncogene family
5.2	6.3	–2.1	4.6×10^{-7}	3.0×10^{-4}	SERPINB5	Serpin peptidase inhibitor, clade B (ovalbumin), member 5
2.3	3.3	–2.1	2.4×10^{-2}	2.3×10^{-1}	CCDC30	Coiled-coil domain containing 30
4.5	5.6	–2.1	1.1×10^{-2}	1.6×10^{-1}	MUC5AC; MUC5B	Mucin 5AC, oligomeric mucus/gel-forming; mucin 5B, oligomeric mucus/gel-forming
6.8	7.8	–2.0	1.2×10^{-5}	2.7×10^{-3}	DCBLD2	Discoidin, CUB and LCCL domain containing 2
3.1	4.2	–2.0	5.1×10^{-6}	1.4×10^{-3}	LYZ	Lysozyme
4.1	5.1	–2.0	6.5×10^{-7}	3.0×10^{-4}	CD33	CD33 molecule
3.8	4.8	–2.0	8.0×10^{-5}	9.7×10^{-3}	IFIT1	Interferon-induced protein with tetratricopeptide repeats 1
1.8	2.8	–2.0	1.0×10^{-3}	4.6×10^{-2}	SPDYE3	Speedy/RINGO cell cycle regulator family member E3
5.1	6.1	–2.0	1.8×10^{-6}	6.0×10^{-4}	TFCP2	Transcription factor CP2
8.1	9.1	–2.0	1.7×10^{-3}	5.9×10^{-2}	KLK6	Kallikrein related peptidase 6
2.2	3.2	–2.0	4.0×10^{-3}	9.4×10^{-2}	MIR626	MicroRNA 626
4.8	5.8	–2.0	3.0×10^{-4}	2.4×10^{-2}	CES1; CES1P1	Carboxylesterase 1; carboxylesterase 1 pseudogene 1
2.6	3.6	–2.0	4.5×10^{-2}	3.1×10^{-1}	MIR548X2	MicroRNA 548x-2
4.7	3.7	2.0	6.6×10^{-5}	8.6×10^{-3}	MIR210HG	MIR210 host gene
9.1	8.1	2.0	2.4×10^{-6}	8.0×10^{-4}	TXNIP	Thioredoxin interacting protein

Table II. *Continued*

Table II. *Continued*

GPI KO Avg (log2)	Ctrl Avg (log2)	Fold change	*p*-Value	FDR *p*-Value	Gene symbol	Description
3.7	2.7	2.0	2.6×10^{-2}	2.4×10^{-1}	MIR4731	MicroRNA 4731
6.1	5.0	2.1	1.4×10^{-5}	3.0×10^{-3}	RILP	Rab interacting lysosomal protein
4.3	3.3	2.1	1.2×10^{-6}	5.0×10^{-4}	ZSCAN12P1	Zinc finger and SCAN domain containing 12 pseudogene 1
5.1	4.0	2.1	1.7×10^{-3}	6.1×10^{-2}	IL2RG	Interleukin 2 receptor, gamma
4.4	3.4	2.1	6.1×10^{-5}	8.1×10^{-3}	LOXL1	Lysyl oxidasx10-like 1
6.1	5.0	2.1	7.6×10^{-7}	4.0×10^{-4}	PIP5K1B	Phosphatidylinositol-4-phosphate 5-kinase, type I, beta
4.5	3.5	2.1	3.3×10^{-3}	8.5×10^{-2}	SULT1A1	Sulfotransferase family 1A member 1
7.7	6.6	2.1	1.5×10^{-5}	3.2×10^{-3}	ZG16B	Zymogen granule protein 16B
8.5	7.5	2.1	4.3×10^{-6}	1.2×10^{-3}	CDH17	Cadherin 17, LI cadherin (liver-intestine)
3.2	2.1	2.1	7.8×10^{-6}	1.9×10^{-3}	SULT1C2P1	Sulfotransferase family 1C member 2 pseudogene 1
6.3	5.3	2.1	8.5×10^{-5}	1.0×10^{-2}	ZBTB38	Zinc finger and BTB domain containing 38
5.4	4.3	2.1	3.2×10^{-7}	2.0×10^{-4}	ADM	Adrenomedullin
3.8	2.8	2.1	3.1×10^{-5}	5.1×10^{-3}	REG4	Regenerating islet-derived family, member 4
7.3	6.2	2.1	4.2×10^{-3}	9.6×10^{-2}	VEGFA	Vascular endothelial growth factor A
5.2	4.1	2.1	6.9×10^{-5}	8.9×10^{-3}	ENO2	Enolase 2 (gamma, neuronal)
7.5	6.4	2.1	1.5×10^{-5}	3.2×10^{-3}	HK2	Hexokinase 2
7.3	6.2	2.1	3.4×10^{-6}	1.0×10^{-3}	ARG2	Arginase 2
6.7	5.6	2.1	4.7×10^{-6}	1.3×10^{-3}	TMEM139	Transmembrane protein 139
3.0	1.9	2.1	7.0×10^{-4}	3.5×10^{-2}	MIR3188	MicroRNA 3188
6.2	5.1	2.1	2.9×10^{-6}	9.0×10^{-4}	PTPRB	Protein tyrosine phosphatase, receptor type, B
5.1	4.0	2.2	1.8×10^{-3}	6.1×10^{-2}	C1orf233	Chromosome 1 open reading frame 233
7.0	5.9	2.2	6.0×10^{-4}	3.2×10^{-2}	RIT1	Ras-like without CAAX 1
6.2	5.1	2.2	1.6×10^{-6}	6.0×10^{-4}	TMEM141	Transmembrane protein 141
5.6	4.5	2.2	2.5×10^{-5}	4.4×10^{-3}	LOC105371592	Atherin-like
4.7	3.6	2.2	2.3×10^{-3}	7.0×10^{-2}	CPEB3	Cytoplasmic polyadenylation element binding protein 3
3.7	2.6	2.2	2.7×10^{-3}	7.6×10^{-2}	NBPF4	Neuroblastoma breakpoint family, member 4
3.2	2.1	2.2	2.2×10^{-7}	1.0×10^{-4}	ANKRD45	Ankyrin repeat domain 45
7.9	6.8	2.2	1.2×10^{-7}	8.2×10^{-5}	ITPK1	Inositol-tetrakisphosphate 1-kinase
3.7	2.5	2.2	6.8×10^{-8}	5.4×10^{-5}	CTSS	Cathepsin S
6.0	4.9	2.2	1.6×10^{-5}	3.2×10^{-3}	DHRS3	Dehydrogenase/reductase (SDR family) member 3
6.0	4.9	2.2	9.9×10^{-3}	1.5×10^{-1}	IRF9	Interferon regulatory factor 9
5.1	3.9	2.2	3.0×10^{-4}	2.4×10^{-2}	NDUFA4L2	NADH dehydrogenase (ubiquinone) 1 alpha subcomplex, 4-like 2
5.6	4.5	2.2	4.9×10^{-7}	3.0×10^{-4}	KLK1	Kallikrein 1
5.8	4.6	2.2	2.0×10^{-4}	2.0×10^{-2}	RASA4B; RASA4	RAS p21 protein activator 4B; RAS p21 protein activator 4
5.3	4.2	2.2	1.4×10^{-5}	3.0×10^{-3}	SMIM24	Small integral membrane protein 24
5.1	3.9	2.2	1.0×10^{-4}	1.2×10^{-2}	SMAD5	SMAD family member 5
5.8	4.6	2.2	1.7×10^{-2}	1.9×10^{-1}	ABCC6P2	ATP binding cassette subfamily C member 6 pseudogene 2
6.5	5.4	2.2	4.5×10^{-3}	1.0×10^{-1}	LINC01207	Long intergenic non-protein coding RNA 1207
7.7	6.5	2.2	3.4×10^{-6}	1.0×10^{-3}	ABCB1	ATP binding cassette subfamily B member 1
8.4	7.2	2.2	1.2×10^{-6}	5.0×10^{-4}	PLOD1	Procollagen-lysine, 2-oxoglutarate 5-dioxygenase 1
7.9	6.7	2.3	3.9×10^{-6}	1.1×10^{-3}	KRT19	Keratin 19, type I
6.9	5.7	2.3	3.0×10^{-4}	2.3×10^{-2}	SECTM1	Secreted and transmembrane 1
4.5	3.3	2.3	2.0×10^{-4}	1.6×10^{-2}	DMGDH	Dimethylglycine dehydrogenase
4.2	3.1	2.3	1.0×10^{-4}	1.3×10^{-2}	EGLN3	Egl-9 family hypoxia-inducible factor 3
5.1	3.9	2.3	2.8×10^{-5}	4.9×10^{-3}	NXPH4	Neurexophilin 4
9.7	8.5	2.3	3.0×10^{-4}	2.1×10^{-2}	NRN1	Neuritin 1
6.9	5.7	2.3	7.3×10^{-10}	1.4×10^{-6}	FAM84A	Family with sequence similarity 84, member A
8.8	7.6	2.3	9.7×10^{-5}	1.1×10^{-2}	PDK1	Pyruvate dehydrogenase kinase, isozyme 1
5.5	4.2	2.3	2.5×10^{-5}	4.4×10^{-3}	SLC6A10P	Solute carrier family 6 (neurotransmitter transporter), member 10, pseudogene
7.5	6.3	2.4	4.6×10^{-3}	1.0×10^{-1}	INSIG2	Insulin induced gene 2
2.5	1.3	2.4	6.0×10^{-4}	3.1×10^{-2}	MIR4678; MINPP1	MicroRNA 4678; multiple inositol-polyphosphate phosphatase 1
7.1	5.8	2.4	1.7×10^{-8}	1.7×10^{-5}	IL33	Interleukin 33

Table II. *Continued*

Table II. *Continued*

GPI KO Avg (log2)	Ctrl Avg (log2)	Fold change	*p*-Value	FDR *p*-Value	Gene symbol	Description
3.4	2.2	2.4	7.2×10^{-3}	1.3×10^{-1}	VTCN1	V-set domain containing T cell activation inhibitor 1
10.5	9.2	2.4	4.2×10^{-5}	6.4×10^{-3}	CYP2S1	Cytochrome P450, family 2, subfamily S, polypeptide 1
4.4	3.1	2.4	3.0×10^{-4}	2.2×10^{-2}	KRTAP5-5	Keratin associated protein 5-5
3.5	2.2	2.4	1.1×10^{-2}	1.6×10^{-1}	IFNA5	Interferon, alpha 5
6.8	5.5	2.4	6.2×10^{-11}	2.0×10^{-7}	SCIN	Scinderin
7.6	6.3	2.4	2.1×10^{-6}	7.0×10^{-4}	ACY3	Aminoacylase 3
7.8	6.5	2.4	6.6×10^{-7}	3.0×10^{-4}	FRRS1	Ferric-chelate reductase 1
6.4	5.1	2.4	4.6×10^{-8}	4.0×10^{-5}	EFNA1	Ephrin-A1
4.2	2.9	2.5	3.7×10^{-3}	9.0×10^{-2}	C6orf222	Chromosome 6 open reading frame 222
7.2	5.9	2.5	1.5×10^{-6}	6.0×10^{-4}	FXYD3	FXYD domain containing ion transport regulator 3
5.0	3.7	2.5	1.5×10^{-5}	3.1×10^{-3}	KCNQ2	Potassium channel, voltage gated KQT-like subfamily Q, member 2
3.0	1.7	2.5	1.5×10^{-2}	1.9×10^{-1}	UGT2B17; UGT2B15	UDP glucuronosyltransferase 2 family, polypeptide B17; UDP glucuronosyltransferase 2 family, polypeptide B15
8.0	6.7	2.5	7.5×10^{-6}	1.9×10^{-3}	CD68	CD68 molecule
4.5	3.2	2.5	3.0×10^{-2}	2.5×10^{-1}	RIMBP3C	RIMS binding protein 3C
8.6	7.3	2.6	6.1×10^{-5}	8.2×10^{-3}	TDP2	Tyrosyl-DNA phosphodiesterase 2
3.1	1.8	2.6	2.2×10^{-3}	6.9×10^{-2}	MIR519A1	MicroRNA 519a-1
7.3	5.9	2.6	6.0×10^{-8}	5.0×10^{-5}	MRGPRE	MAS-related GPR, member E
3.9	2.5	2.6	6.1×10^{-6}	1.6×10^{-3}	CATSPERB	Catsper channel auxiliary subunit beta
6.6	5.2	2.6	3.9×10^{-3}	9.2×10^{-2}	CA9	Carbonic anhydrase IX
5.8	4.4	2.6	1.4×10^{-8}	1.5×10^{-5}	MAGEA3	MAGE family member A3
8.2	6.8	2.6	3.0×10^{-4}	2.1×10^{-2}	NEAT1	Nuclear paraspeckle assembly transcript 1 (non-protein coding)
7.2	5.8	2.6	4.5×10^{-8}	4.0×10^{-5}	TINAGL1	Tubulointerstitial nephritis antigen-like 1
6.5	5.1	2.7	4.8×10^{-5}	7.1×10^{-3}	BHLHE40	Basic helix-loop-helix family, member e40
6.0	4.6	2.7	3.0×10^{-4}	2.3×10^{-2}	MT1F	Metallothionein 1F
5.0	3.6	2.7	4.0×10^{-7}	2.0×10^{-4}	FBXO17	F-box protein 17
7.5	6.0	2.7	1.3×10^{-6}	5.0×10^{-4}	MT1H	Metallothionein 1H
7.5	6.1	2.7	1.4×10^{-10}	3.8×10^{-7}	PAQR5	Progestin and adipoQ receptor family member V
4.2	2.8	2.7	1.7×10^{-5}	3.3×10^{-3}	LINC00967	Long intergenic non-protein coding RNA 967
5.0	3.5	2.8	2.0×10^{-7}	1.0×10^{-4}	DAB2; C9	Dab, mitogen-responsive phosphoprotein, homolog 2 (Drosophila); complement component 9
4.8	3.3	2.8	3.0×10^{-4}	2.4×10^{-2}	C17orf77	Chromosome 17 open reading frame 77
8.0	6.5	2.9	2.6×10^{-6}	8.0×10^{-4}	SNORA75	Small nucleolar RNA, H/ACA box 75
8.0	6.5	2.9	5.0×10^{-4}	3.0×10^{-2}	GBE1	Glucan (1,4-alpha-), branching enzyme 1
4.5	3.0	2.9	5.0×10^{-4}	3.0×10^{-2}	TDGF1	Teratocarcinoma-derived growth factor 1
6.7	5.1	2.9	2.9×10^{-7}	2.0×10^{-4}	RNF144A	Ring finger protein 144A
6.2	4.6	3.0	7.7×10^{-7}	4.0×10^{-4}	BAAT	Bile acid-CoA:amino acid N-acyltransferase
7.3	5.7	3.0	5.1×10^{-7}	3.0×10^{-4}	KDM3A	Lysine (K)-specific demethylase 3A
7.2	5.6	3.0	5.6×10^{-8}	4.7×10^{-5}	FAM13A	Family with sequence similarity 13, member A
8.0	6.4	3.1	9.8×10^{-9}	1.2×10^{-5}	ANPEP	Alanyl (membrane) aminopeptidase
7.2	5.5	3.1	8.8×10^{-5}	1.0×10^{-2}	ALDOC	Aldolase C, fructosx10-bisphosphate
4.5	2.9	3.1	1.3×10^{-9}	2.3×10^{-6}	MUC3A; MUC3B	Mucin 3A, cell surface associated; mucin 3B, cell surface associated
10.5	8.9	3.1	4.5×10^{-6}	1.2×10^{-3}	PIGR	Polymeric immunoglobulin receptor
6.3	4.7	3.1	3.0×10^{-2}	2.5×10^{-1}	SPINK1	Serine peptidase inhibitor, Kazal type 1
8.7	7.0	3.1	6.5×10^{-5}	8.6×10^{-3}	PLOD2	Procollagen-lysine, 2-oxoglutarate 5-dioxygenase 2
9.6	7.9	3.1	1.3×10^{-5}	2.8×10^{-3}	SLC2A1	Solute carrier family 2 (facilitated glucose transporter), member 1
6.1	4.5	3.1	4.2×10^{-9}	5.9×10^{-6}	CDA	Cytidine deaminase
6.7	5.0	3.1	5.0×10^{-4}	2.9×10^{-2}	FUT11	Fucosyltransferase 11 (alpha (1,3) fucosyltransferase)
8.3	6.6	3.1	8.7×10^{-5}	1.0×10^{-2}	SLC6A19	Solute carrier family 6 (neutral amino acid transporter), member 19
10.3	8.6	3.2	1.8×10^{-6}	6.0×10^{-4}	BNIP3	BCL2/adenovirus E1B 19kDa interacting protein 3
9.3	7.6	3.2	1.0×10^{-4}	1.2×10^{-2}	P4HA1	Prolyl 4-hydroxylase, alpha polypeptide I
7.1	5.4	3.3	5.4×10^{-6}	1.4×10^{-3}	PFKFB3	6-phosphofructo-2-kinase/fructosx10-2,6-biphosphatase 3

Table II. *Continued*

Table II. *Continued*

GPI KO Avg (log2)	Ctrl Avg (log2)	Fold change	*p*-Value	FDR *p*-Value	Gene symbol	Description
5.7	4.0	3.3	1.4×10^{-8}	1.5×10^{-5}	GUCY2C	Guanylate cyclase 2C
6.3	4.6	3.3	2.7×10^{-7}	2.0×10^{-4}	ANKRD37	Ankyrin repeat domain 37
6.6	4.9	3.3	9.4×10^{-9}	1.2×10^{-5}	PMP22	Peripheral myelin protein 22
5.7	3.9	3.3	1.7×10^{-7}	1.0×10^{-4}	BTNL3	Butyrophilin-like 3
5.0	3.3	3.4	1.2×10^{-3}	5.0×10^{-2}	LRRC19	Leucine rich repeat containing 19
8.0	6.2	3.4	2.6×10^{-7}	2.0×10^{-4}	ARRDC4	Arrestin domain containing 4
5.6	3.9	3.4	7.4×10^{-9}	9.6×10^{-6}	PPARGC1A	Peroxisome proliferator-activated receptor gamma, coactivator 1 alpha
6.6	4.8	3.4	5.4×10^{-7}	3.0×10^{-7}	TFF3	Trefoil factor 3
6.1	4.3	3.5	1.0×10^{-7}	7.3×10^{-5}	RHOBTB3	Rho-related BTB domain containing 3
6.8	5.0	3.6	5.0×10^{-4}	2.8×10^{-2}	SULT1C2	Sulfotransferase family 1C member 2
5.8	4.0	3.6	1.0×10^{-8}	1.2×10^{-5}	CPXM2	Carboxypeptidase X (M14 family), member 2
5.8	3.9	3.6	1.9×10^{-10}	4.7×10^{-7}	S100A9	S100 calcium binding protein A9
6.9	5.1	3.7	1.5×10^{-11}	6.2×10^{-8}	SEMA6A	Sema domain, transmembrane domain (TM), and cytoplasmic domain, (semaphorin) 6A
4.8	2.9	3.7	1.9×10^{-6}	7.0×10^{-4}	PAG1	Phosphoprotein membrane anchor with glycosphingolipid microdomains 1
6.9	4.9	3.8	1.6×10^{-3}	5.9×10^{-2}	C6orf223	Chromosome 6 open reading frame 223
6.9	4.9	3.9	1.1×10^{-8}	1.3×10^{-5}	FXYD4	FXYD domain containing ion transport regulator 4
9.5	7.5	3.9	2.0×10^{-4}	1.5×10^{-2}	TFF1	Trefoil factor 1
4.9	2.9	4.1	1.6×10^{-5}	3.3×10^{-3}	TGFBI	Transforming growth factor, beta-induced, 68kDa
9.0	6.8	4.3	2.1×10^{-5}	4.0×10^{-3}	LCN15	Lipocalin 15
7.2	5.1	4.4	1.2×10^{-6}	5.0×10^{-6}	TFF2	Trefoil factor 2
5.1	2.9	4.6	1.0×10^{-6}	4.0×10^{-4}	TMEM45A	Transmembrane protein 45A
5.5	3.2	4.9	8.3×10^{-12}	5.0×10^{-8}	MUC17	Mucin 17, cell surface associated
7.2	5.0	4.9	2.6×10^{-3}	7.5×10^{-2}	IL37	Interleukin 37
5.2	2.7	5.4	1.2×10^{-6}	5.0×10^{-4}	CASP5	Caspase 5
6.8	4.3	5.9	6.7×10^{-6}	1.7×10^{-3}	NDRG1	N-myc downstream regulated 1
7.0	4.0	8.1	1.4×10^{-14}	1.7×10^{-10}	IRF8	Interferon regulatory factor 8
9.9	6.7	8.8	5.8×10^{-9}	7.8×10^{-6}	HMGCS2	3-hydroxy-3-methylglutaryl-CoA synthase 2 (mitochondrial)
6.3	3.0	9.5	2.2×10^{-10}	5.1×10^{-7}	HTR1D	5-hydroxytryptamine (serotonin) receptor 1D, G protein-coupled
6.9	3.3	11.9	1.4×10^{-3}	5.4×10^{-2}	LOC105378283	Putative ankyrin repeat domain-containing protein ENSP00000383069
9.1	4.2	29.5	1.3×10^{-6}	5.0×10^{-4}	KIT	v-kit Hardy-Zuckerman 4 feline sarcoma viral oncogene homolog
9.4	3.2	72.2	9.4×10^{-18}	4.5×10^{-13}	S100A7	S100 calcium binding protein A7

(ACC) (which decreases malonyl-CoA), causing the release of carnitine palmitoyltransferase 1A (CPT-1A), aiding the transport of fatty-acyl chains to mitochondria for β-oxidation (25-27). Theoretically, glycolysis would trigger elevation in *PGC-1α*, where this metabolic fuel switch should coincide with attenuation of biosynthesized steroids and cholesterol, where inactivation of HMG-CoA reductase (HMGCR) would then enable HMG-CoA to be rerouted to the production of ketones (this involving HMGCS2), both elevated in the KO clones. If this was the case, ketones [β-hydroxybutyrate (bHB), acetoacetate, acetone] would be produced through 2 or more acetyl-CoA molecules being condensed by the following enzymes: acetoacetyl-CoA thiolase (ACAT1), HMGCS2 and HMG-CoA lyase (HMGC). We did a follow up investigation for the presence of bHB and acetoacetate, finding no evidence of accumulation of both of these ketones (data not shown). Ketones, if present could be used to fuel the TCA cycle, through the reverse conversion of bHB to acetoacetate, then converted to acetoacetyl-CoA (by succinyl-CoA:3-ketoacid-CoA transferase, SCOT) and lastly to Acetyl-CoA by ACAT1. The end goal of a metabolic flip switch would be to regulate sources of acetyl-CoA to fuel the TCA cycle from glucose (during a fed state) to fats in a non-fed state (β-oxidation). Another metabolic reprogramming gene that was elevated in both KO clones was *acetyl-CoA acyltransferase 2* (*ACAA2*).

Future work will be required to corroborate if what we are seeing in both KOs is similar to lipid metabolic oncogenic

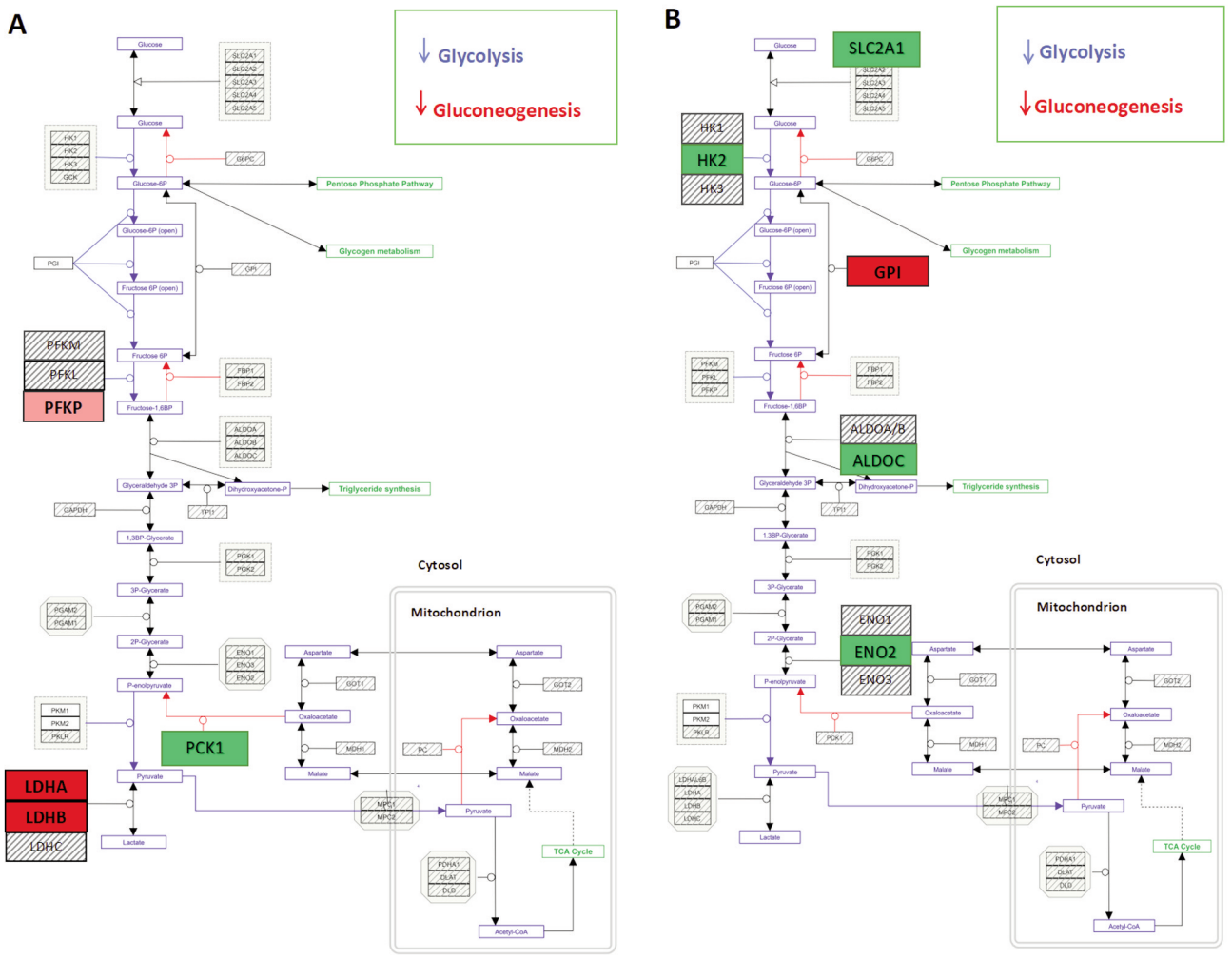

Figure 4. *(A) Wiki Pathway analysis of LDHA/B DKO DEF changes observed in glycolysis, gluconeogenesis and mitochondrial TCA cycle pathways. (B) Wiki Pathway analysis of GPI KO DEF changes observed in glycolysis, gluconeogenesis and mitochondrial TCA cycle pathways. In red are the down-regulated transcripts and in green the up-regulated transcripts. Filtered by fold change <-2 or >2, p-Value<0.05.*

reprogramming described in diverse cancers which involve the overexpression of both *HMGC2* (28, 29) and *PGC-1α* transcripts (24). Overexpression of *HMGC2/PGC-1α* has been observed in high-grade colorectal cancer (30), colitis-associated cancer (31), clear cell renal cell cancer (32, 33), ovarian (34), liver (35), oral squamous cell carcinoma (36) and high-grade prostate cancer (37), and is reflective of recurrence and poor prognosis (38). The dual induction of *HMGCS2/PGC-1α* also propels oncogenic mediated ketogenic events within the cancer milieu/stroma (for example, in cancer-associated fibroblasts) (39).

Increase in thioredoxin interacting protein transcripts (TXNIP). Concomitant changes to glycolysis in both KOs were few, but the elevated expression of *TXNIP* was however notable (40). This is a pathological feature of type II diabetes and biological tissues that are unable to utilize glucose (glucose intolerance) (41). An earlier work with a fibroblast mutant defective in phosphoglucose isomerase (*PGI*) demonstrated that glucose-6-phosphate is the key accumulated metabolite "repressing" glucose transport activity (42), a mechanism further elucidated by Ayer's group in which TXNIP was shown to be induced through a nuclear transcription factor complex, ChREBP/Mlx, (MondoA-Mlx) (43). Finally, TXNIP, by direct interaction with GLUT1 transporter stops its activity by internalization through clathrin coated pits (44). Research using diverse models show a reciprocal self-perpetuated elevation in TXNIP, resulting in the inability to use glucose, with elevated glucose levels driving then further expression of TXNIP (40). The rise in TXNIP,

Table III. *DEG patterns in both KO clones relative to WT Controls*.

DEG patterns in both KO clones relative to WT Controls		Effects in LDHA/B DKO			Effects in GPI KO		
Gene symbol	Description	FC	*p*-Value	FDR *p*-Value	FC	*p*-Value	FDR *p*-Value
MUC6	Mucin 6, oligomeric mucus/ gel-forming	-15.5	2.8×10^{-12}	1.0×10^{-8}	-2.3	1.3×10^{-2}	1.7×10^{-1}
DKK4	Dickkopf WNT signaling pathway inhibitor 4	-11.0	7.5×10^{-8}	3.5×10^{-5}	-20.6	2.1×10^{-8}	2.0×10^{-5}
BGN	Biglycan	-7.3	1.0×10^{-4}	1.2×10^{-2}	-8.4	3.0×10^{-4}	2.2×10^{-2}
DSC3	Desmocollin 3	-5.7	1.7×10^{-12}	9.0×10^{-9}	-5.9	1.0×10^{-11}	5.3×10^{-8}
CRYBB1	Crystallin beta B1	-5.6	8.2×10^{-7}	2.0×10^{-4}	-3.1	2.0×10^{-4}	1.5×10^{-2}
AKR1C2	Aldo-keto reductase family 1, member C2	-5.4	1.2×10^{-9}	1.4×10^{-6}	-7.6	2.5×10^{-10}	5.5×10^{-7}
AKR1B10	Aldo-keto reductase family 1, member B10 (aldose reductase)	-4.7	1.9×10^{-13}	4.7×10^{-9}	-3.4	1.3×10^{-10}	3.7×10^{-7}
HULC	Hepatocellular carcinoma up-regulated long non-coding RNA	-3.8	1.7×10^{-6}	4.0×10^{-4}	-3.9	5.6×10^{-6}	1.5×10^{-3}
BCL11A	B-cell CLL/lymphoma 11A (zinc finger protein)	-3.5	2.8×10^{-10}	4.3×10^{-7}	-2.3	2.5×10^{-6}	8.0×10^{-4}
HUNK	Hormonally up-regulated Neu-associated kinase	-3.4	3.5×10^{-6}	7.0×10^{-4}	-4.2	6.3×10^{-7}	3.0×10^{-4}
THSD4	Thrombospondin type 1 domain containing 4	-3.3	7.0×10^{-9}	5.7×10^{-6}	-2.9	1.3×10^{-7}	8.8×10^{-5}
HBE1	Hemoglobin, epsilon 1	-3.2	1.4×10^{-5}	2.0×10^{-3}	-3.2	5.0×10^{-6}	1.4×10^{-3}
CALB2	Calbindin 2	-3.1	2.9×10^{-5}	3.6×10^{-3}	-7.8	1.4×10^{-6}	5.0×10^{-4}
ALDH3A1	Aldehyde dehydrogenase 3 family, member A1	-3.0	3.7×10^{-6}	8.0×10^{-4}	-3.6	7.4×10^{-6}	1.8×10^{-3}
FGFBP1	Fibroblast growth factor binding protein 1	-2.9	5.4×10^{-7}	2.0×10^{-4}	-2.1	2.2×10^{-5}	4.0×10^{-3}
OR51B4	Olfactory receptor, family 51, subfamily B, member 4	-2.7	7.0×10^{-4}	3.4×10^{-2}	-3.1	5.0×10^{-4}	3.0×10^{-2}
EIF2B5-AS1	EIF2B5 antisense RNA 1	-2.7	6.0×10^{-4}	2.9×10^{-2}	-3.9	1.3×10^{-5}	2.9×10^{-3}
GPX2	Glutathione peroxidase 2	-2.7	1.5×10^{-5}	2.2×10^{-3}	-4.5	1.8×10^{-6}	6.0×10^{-4}
GPX8	Glutathione peroxidase 8 (putative)	-2.7	6.3×10^{-7}	2.0×10^{-4}	-2.5	3.1×10^{-6}	1.0×10^{-3}
ANOS1	Anosmin 1	-2.7	5.3×10^{-9}	4.6×10^{-6}	-2.6	2.1×10^{-8}	2.0×10^{-5}
SLC7A11	Solute carrier family 7 (AA transporter LC, xc- system), member 11	-2.7	8.5×10^{-6}	1.4×10^{-3}	-2.3	7.5×10^{-5}	9.2×10^{-3}
VCAN	Versican	-2.7	9.7×10^{-3}	1.6^{X10-1}	-10.7	1.3×10^{-5}	2.8×10^{-3}
TFCP2	Transcription factor CP2	-2.7	2.6×10^{-9}	2.7×10^{-6}	-2.0	1.8×10^{-6}	6.0×10^{-4}

Table III. *Continued*

Table III. *Continued*

DEG patterns in both KO clones relative to WT Controls		Effects in LDHA/B DKO			Effects in GPI KO		
Gene symbol	Description	FC	*p*-Value	FDR *p*-Value	FC	*p*-Value	FDR *p*-Value
CES1; CES1P1	Carboxylesterase 1; carboxylesterase 1 pseudogene 1	-2.6	5.5×10^{-6}	1.0×10^{-3}	-2.0	3.0×10^{-4}	2.4×10^{-2}
ALDH1A1	Aldehyde dehydrogenase 1 family, member A1	-2.6	1.1×10^{-8}	7.8×10^{-6}	-2.8	2.0×10^{-8}	2.0×10^{-5}
LYZ	Lysozyme	-2.6	1.8×10^{-8}	1.2×10^{-5}	-2.0	5.1×10^{-6}	1.4×10^{-3}
CORO1A	Coronin, actin binding protein, 1A	-2.2	1.0×10^{-4}	9.6×10^{-3}	-2.1	3.0×10^{-3}	8.0×10^{-2}
PLA2G16	Phospholipase A2, group XVI	-2.2	7.0×10^{-9}	5.7×10^{-6}	-2.5	3.0×10^{-9}	4.5×10^{-6}
AKR1C1	Aldo-keto reductase family 1, member C1	-2.1	6.4×10^{-6}	1.1×10^{-3}	-2.5	6.6×10^{-7}	3.0×10^{-4}
HOXB9	Homeobox B9	-2.1	5.2×10^{-6}	1.0×10^{-3}	-4.7	5.0×10^{-11}	1.7×10^{-7}
SERPINB5	Serpin peptidase inhibitor, clade B (ovalbumin), member 5	-2.1	1.4×10^{-7}	5.7×10^{-5}	-2.1	4.6×10^{-7}	3.0×10^{-4}
GXYLT2	Glucoside xylosyltransferase 2	-2.1	2.1×10^{-6}	5.0×10^{-4}	-2.2	2.7×10^{-6}	9.0×10^{-4}
APCDD1	Adenomatosis polyposis coli down-regulated 1	-2.0	7.3×10^{-6}	1.3×10^{-3}	-5.7	1.7×10^{-10}	4.3×10^{-7}
ACAA2	Acetyl-CoA acyltransferase 2	1.7	9.2×10^{-7}	2.0×10^{-4}	1.7	1.2×10^{-5}	2.7×10^{-3}
TXNIP	Thioredoxin interacting protein	2.0	4.4×10^{-8}	2.3×10^{-5}	2.0	2.4×10^{-6}	8.0×10^{-4}
LYST	Lysosomal trafficking regulator	2.0	2.6×10^{-3}	7.8×10^{-2}	2.3	1.4×10^{-5}	2.1×10^{-3}
ARRDC4	Arrestin domain containing 4	2.1	3.0×10^{-6}	6.0×10^{-4}	3.4	2.6×10^{-7}	2.0×10^{-4}
SECTM1	Secreted and transmembrane 1	2.2	1.8×10^{-5}	2.5×10^{-3}	2.3	3.0×10^{-4}	2.3×10^{-2}
C6orf222	Chromosome 6 open reading frame 222	2.3	3.0×10^{-4}	2.0×10^{-2}	2.5	3.7×10^{-3}	9.0×10^{-2}
HMGCS2	3-hydroxy-3-methylglutaryl-CoA synthase 2 (mitochondrial)	2.4	5.4×10^{-6}	1.0×10^{-3}	8.8	5.8×10^{-9}	7.8×10^{-6}
ZSCAN12P1	Zinc finger and SCAN domain containing 12 pseudogene 1	2.5	3.6×10^{-8}	2.0×10^{-5}	2.1	1.2×10^{-6}	5.0×10^{-4}
SEMA6A	Sema domain, trans mem (TM), cytoplasmic , (semaphorin) 6A	2.6	5.2×10^{-10}	7.2×10^{-7}	3.7	1.5×10^{-11}	6.2×10^{-8}
SNORA75	Small nucleolar RNA, H/ACA box 75	2.7	1.1×10^{-7}	4.7×10^{-5}	2.9	2.6×10^{-6}	8.0×10^{-4}
CD68	CD68 molecule	3.3	9.2×10^{-8}	4.2×10^{-5}	2.5	7.5×10^{-6}	1.9×10^{-3}
PPARGC1A	Peroxisome proliferator-activated receptor gamma, coactivator 1 alpha	3.4	3.8×10^{-10}	5.4×10^{-7}	3.4	7.4×10^{-9}	9.6×10^{-6}
IRF9	Interferon regulatory factor 9	4.3	1.5×10^{-8}	1.1×10^{-5}	2.2	9.9×10^{-3}	1.5×10^{-1}
FXYD4	FXYD domain containing ion transport regulator 4	4.7	1.3×10^{-10}	2.3×10^{-7}	3.9	1.1×10^{-8}	1.3×10^{-5}
SPINK1	Serine peptidase inhibitor, Kazal type 1	5.6	2.0×10^{-4}	1.3×10^{-2}	3.1	3.0×10^{-2}	2.5×10^{-1}

besides a reduction in glucose uptake, can lead to reduced glycolytic enzyme activities (such as Phosphofructokinase, Pyruvate Kinase and Lactate Dehydrogenase), the Pentose phosphate pathway (PPP) and Glucose-6-Phosphate Dehydrogenase (45). This is entirely opposite in cancer, where a reported loss of TXNIP correlates to the observed *Warburg effect*: rapid glycolysis, higher glucose uptake, and activation of glutaminolysis (46, 47). In other words, diabetes is a disease involving higher TXNIP expression with the inability to use glucose, while cancer is a disease corresponding to lower TXNIP and heightened ability to use glucose, particularly with regards to glycolysis.

Reduction in aldehyde dehydrogenase transcripts (ALDHs) One of the most significant losses in response to glycolytic impairment in both KO clones was the concomitant repression of several aldehyde dehydrogenase transcripts, specifically *ALDH1A1*, *ALDH2* (mitochondrial), and *ALDH3A1*, which could create a *non-ergogenic* vulnerability to cancer cells. High expression of these genes is observed in many cancers, playing a critical role in the biosynthesis of retinoic acid (RA), nuclear signaling (48, 49) and contribution toward the "stemness" or self-renewal features which perpetuates tumor initiation and drug/radiation resistance (50-54). While ALDHs are keys in the collective stemness gene profile (*CSN6*, *CD15*, *CD24*, *CD166*, *TRIM21*, *CD133*, *CD82*, *CD105*, *CD44*, *CD90*, *ALDH1A1*, *EPCAM*, *SOX2*, *SOX9*, *LGR5*, *BMI1*, *NANOG*, *OCT4*, *CXCR4* and *CD24*), ALDHs are specifically up-regulated by pro-oncogenic proteins such as cytokines, growth factors or pollutants which trigger epithelial-mesenchymal transition (EMT), colony formation, migration, and metastasis in diverse cancers with poor clinical outcome (55-61).

One of the critical questions that comes to mind from this particular aspect of the data is the following: is there a correlation between the reduction in ALDHs and metabolic reprogramming? While few studies have investigated this aspect, there are reports suggesting that, in adipocytes, the observed overexpression of ALDH1A1 is associated with fatty acid synthesis, obesity, insulin resistance (62) as well as lipogenesis and triglyceride production (63). In cancer tissues, the rise in ALDHs is associated with heightened glucose uptake, activation of the glycolytic pathway, and elevation of GLUT1 (64). While the loss of ALDHs coincides with complete loss of glucose utilization in both KO clones, the causal effect, if any, between these two events will need further investigation. Future studies will be needed to confirm if LDHA/B inhibitors could be combined with ALDH inhibitors to evoke a more significant chemotherapeutic effect of drugs and radiation (48), and could be explored with ALDH inhibitors such as (–)-epigallocatechin gallate (65, 66), rocaglamide A (67), NCT-501 (67), and ellagic acid (68).

Reduction in Aldo-keto reductase (AKR) transcripts. In this work, we also see a consistent downregulation of several *ARKs*, including *AKR1B10*, *AKR1C1*, *AKR1C2* and *AKR1C3* in both KO clones. Higher expression of *ARKS* is frequently reported in cases of liver damage due to environmental pollutants (69), hepatitis C and B virus, aflatoxin B1 (70-72), nonalcoholic fatty liver, steatohepatitis (73), fibrosis (74), and cirrhosis (75). The ARKs, including *AKR1B10* and *AKR1C3*, are also overexpressed in a number of premalignant and established cancers including liver cancer (76-78), and play a role in prostanoid synthesis which drives hormone-dependent cancers including prostate, breast, and endometrial ones (79-81). Heightened *AKR1B10* overexpression is also critical to cancers associated with protein prenylation of mutant KRAS; which is a formidable prognostic indicator to tumor invasion, metastasis and progression (82-84), chemoresistance (85), radiation resistance (86), recurrence, tumor size and overall poor clinical outcomes (87-89). Downregulation of *ARK1B10* observed in both glycolysis-null clones would favor a vulnerability to tumor growth. This has been shown many times, through either KO or inhibition of AKR1B10 in various *in vitro* and *in vivo* models which demarcates reduced tumor growth, metastasis (90, 91), protein prenylation (92), colony formation (3), and ultimately more significant response to chemotherapy drugs such as doxorubicin (93). Given this role in cancer, future research could be conducted to examine if there is a synergistic effect when using LDHA/B inhibitors and ARK class inhibitors, such as apigenin, luteolin (94), epalrestat (95), hop-derived compounds (adhumulone), n-humulone (96), xanthohumol isoxanthohumol (97), caffeic acid phenethyl esters, tolrestat, zopolrestat, sorbinil (76), curcumin, magnolol honokiol (16), oleanolic acid (76) and baccharin analogs or sulfonylureas (98).

WNT signaling. One of the most significant differential shifts in both KOs was the reduced expression of inhibitory controls over WNT signaling: loss of *DKK4* (-20.53 FC), which otherwise would act as a canonical WNT/β-catenin signaling inhibitor. In the *GPI* KO, this corresponded to a significant elevation of *C-KIT* (+29.65 FC), a major driving force in WNT/β-catenin signaling which plays a role in cancer stem cell reprogramming, EMT, immune evasion and drug resistance (99, 100). The effects of enhanced WNT

→

Figure 5. *(A) Wiki Pathway analysis of LDHA/B DKO DEF changes observed in integrated amino acid metabolic pathways. (B) Wiki Pathway analysis of GPI KO DEF changes observed in integrated amino acid metabolic pathways. In red are the down-regulated transcripts and in green the up-regulated transcripts. Filtered by fold change <-2 or >2, p-Value<0.05.*

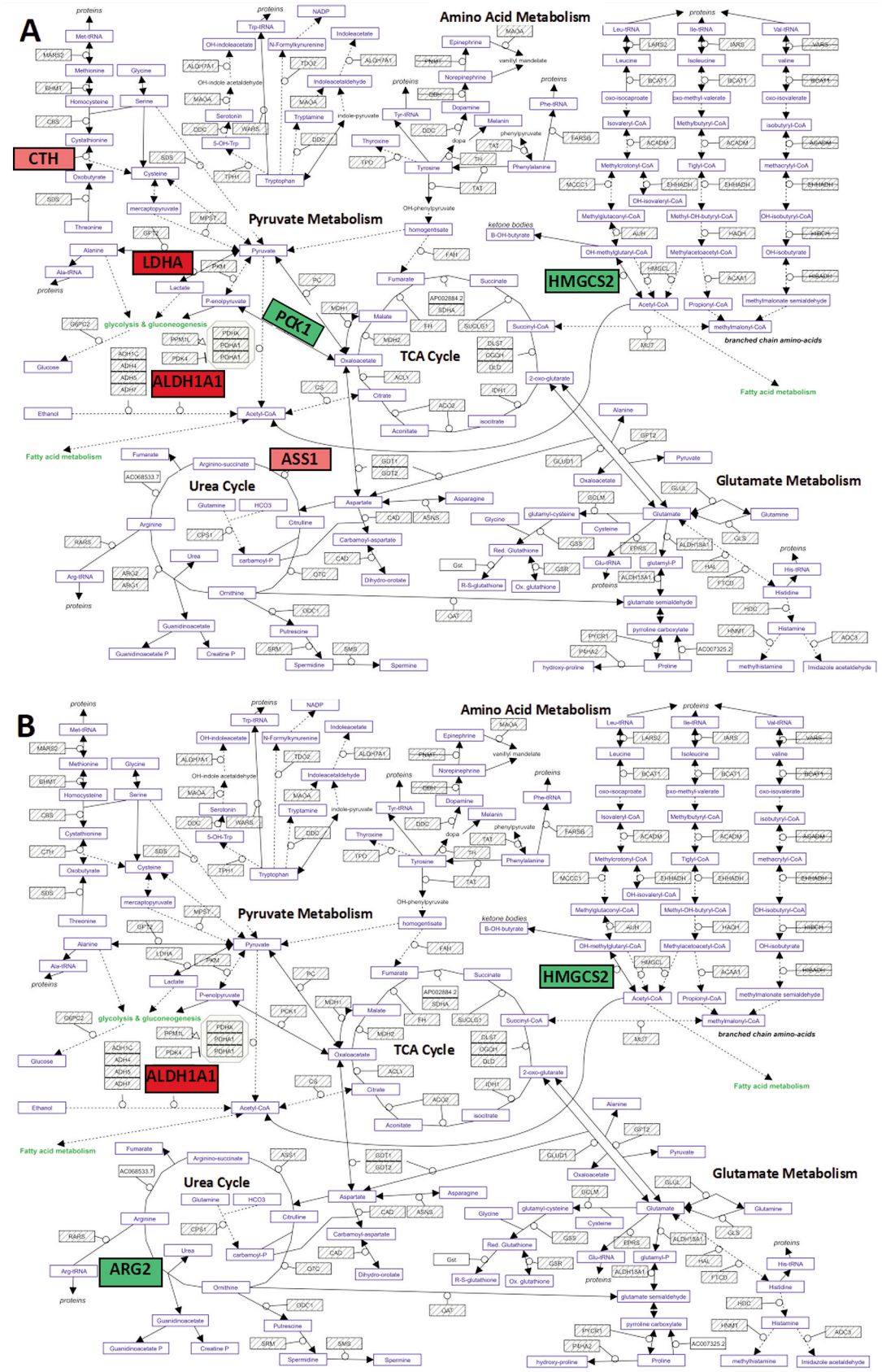
A
CTH
LDHA
PCK1
ALDH1A1
ASS1
HMGCS2
Amino Acid Metabolism
Pyruvate Metabolism
TCA Cycle
Urea Cycle
Glutamate Metabolism
glycolysis & gluconeogenesis
branched chain amino-acids
Fatty acid metabolism
ketone bodies
B
ARG2

signaling on glycolysis-null cells would definitely deserve further investigation.

Normally, DKK4 acts to suppress the canonical WNT signaling as follows. Briefly, canonical WNT signaling is initiated by WNT ligands that bind to Frizzled (Fzd) receptor family, and cytoplasmic low-density-lipoprotein-related protein 5/6 (LRP5/6, the binding target of DKK4) (101, 102). If DKK inhibits this mechanism, then it would prevent the phosphorylation, recruitment, and polymerization of Dishevelled (Dvl), that would otherwise bind axin to the receptor and inactivate the β-catenin destruction complex. When activated, this leads to a subsequent rise in β-catenin levels which precipitates its translocation into the nucleus to interact with transcription factors [T-cell factor (TCF) and lymphoid enhancer factor (LEF)] to promote cell proliferation and tumorigenesis (103). Both KOs also displayed reduced expression of *APC down-regulated 1* (*APCDD1*), which also binds to WNT3a/LRP5 (102, 104) and inhibits WNT/β-catenin LEF transcriptional signaling (105, 106). The attenuation of negative WNT controls (*APCDD1* and *DKK4*) in glycolytic KOs would, in theory, lead to a rise in β-catenin, which, if occurring in the cytoplasm, could interact with cadherin, bind to the actin filaments or TGF-β and alter cell-cell adhesion, thus resulting in a very loose mesenchymal phenotype contributing to metastasis. This could be a negative consequence, particularly for colon cancer, since high catenin levels, coinciding with inability of proteolytic degradation of β-catenin as in the case of mutations in *TrCP1* (*β-TrCP*) *E3 ubiquitin ligase* motifs or *β-catenin* recruiting motifs of adenomatous polyposis coli (APC) can lead to precancerous polyps with the capacity to transform into lethal tumors (107).

However, it is important to note that concerning DKK4, there is a remarkable inconsistency in regard to its effect on WNT signaling. While many reports reveal its tumor suppressor role, it is also reported to be overexpressed in diverse cancers, corresponding to tumorigenesis and metastasis (108) including esophageal cancer (109), endometrial cancer and thyroid carcinoma (110, 111). While healthy tissue is devoid of DKKs, elevated DKK expression is found in matched tumor tissues (112) and overexpressed chemoresistant (113, 114) and metastatic xenograft models of CRC (115). Further confounding its role, a reduction in DKK4, either experimentally manipulated or inherent, corresponds to increased β-catenin-mediated transcriptional activity on target genes including *Axin2* and *CCND1* (116), which drive proliferation (117). While several research groups are looking into this paradox, it is believed that pro-tumoral properties of DKK may be attributable to activating a non-canonical c-Jun N-terminal kinase (JNK) signaling pathway while inhibiting the WNT-canonical pathway (118).

Future research will be required to evaluate the synergistic effects of LDHA/B inhibitors with a diverse range of drugs that target WNT signaling. C-KIT can be inhibited by drugs such as imatinib or mastinib which down-regulate stem cell markers, enhance the therapeutic efficacy of cytostatic agents (119), and prevent its role in the stroma to promote tumorigenesis, angiogenesis, proliferation and survival (120, 121).

Extracellular matrix (ECM). One of the most striking visual observations to the morphology of the knockouts was the loss of cell-cell adhesion relative to WT in both KO clones, also reflected by a significant loss of genes controlling cell-cell/cell – surface or ECM systems. Some of these included losses to ECM component genes which would otherwise play a role in cancer migration, motility and invasion, such as *Anosmin 1* or *Biglycan* (122-125). The type of losses in ECM anchoring related genes as shown in this study (such as *VCAN*) could evoke the remodeling of tumor stroma matrix which is known to enable sequestration of tumor-promoting immune cells and angiogenesis (126-128). Combined with losses in *desmocollin 3* (129, 130) and *moesin* (*MSN*) (131), it could then worsen EMT and metastasis (132).

In summary, this work provides an overall broad layout of the transcriptomic changes that are triggered by severe compromise to glycolysis by KO of *LDHA/B* or *GPI* genes, specific to this highly aggressive type of colon cancer. Future research will be required to clearly demarcate all plausible ergogenic pathways in tumor cells to identify a multi-target tumor-specific approach to destroy the tumor metabolic requirements.

Availability of Data and Material

The dataset has been deposited to NIH Gene Expression Omnibus located at: https://www.ncbi.nlm.nih.gov/geo/query/acc.cgi?acc=GSE149289.

Conflicts of Interest

The Authors declare that they have no conflicts of interest.

Authors' Contributions

EM carried out the basic metabolic profiling and microarray work. RB assisted with daily tasks and consultation on experimental design and troubleshooting. NM assisted with ATP assays. KS oversaw this project from start to finish by scientific consultation, guidance, manuscript preparation and review. ZM isolated and characterized the two glycolytic-null cell lines. SC has done cell growth, viability, clonogenic assays and assisted manuscript preparation and edition. JP oversaw this collaborative project by scientific consultation, guidance and review.

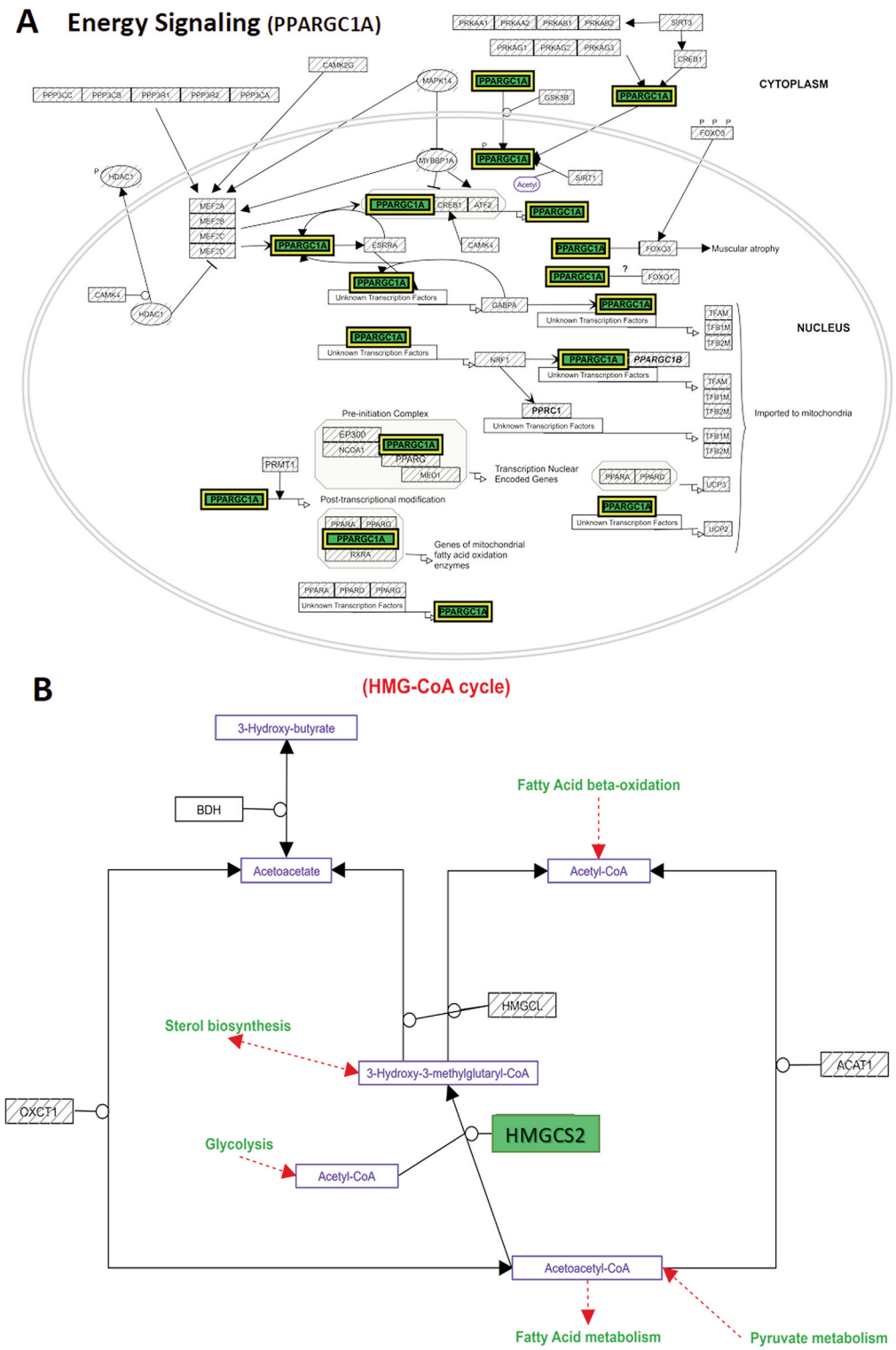

Figure 6. *(A) Wiki Pathway analysis of overlapping upregulated DEG changes observed in both LDHA/B DKO and GPI KO in energy pathways. The PPARGC1A differential transcript changes were as follows: WT versus LDHA/B DKO: (FC +3.43, FDR p-Value<0.001); WT versus GPI KO: (FC +3.39, FDR p-Value <0.001). (B) Wiki Pathway analysis of overlapping up-regulated DEF changes observed in both LDHA/B DKO and GPI KO in the HMG-CoA pathway. The HMGCS2 differential transcript changes were as follows: WT versus LDHA/B DKO: (FC +3.43, FDR p-Value<0.001); WT versus GPI KO: (FC +3.39, FDR p-Value<0.001). In red are the down-regulated transcripts and in green the up-regulated transcripts. Filtered by fold change <-2 or >2, p-Value<0.05.*

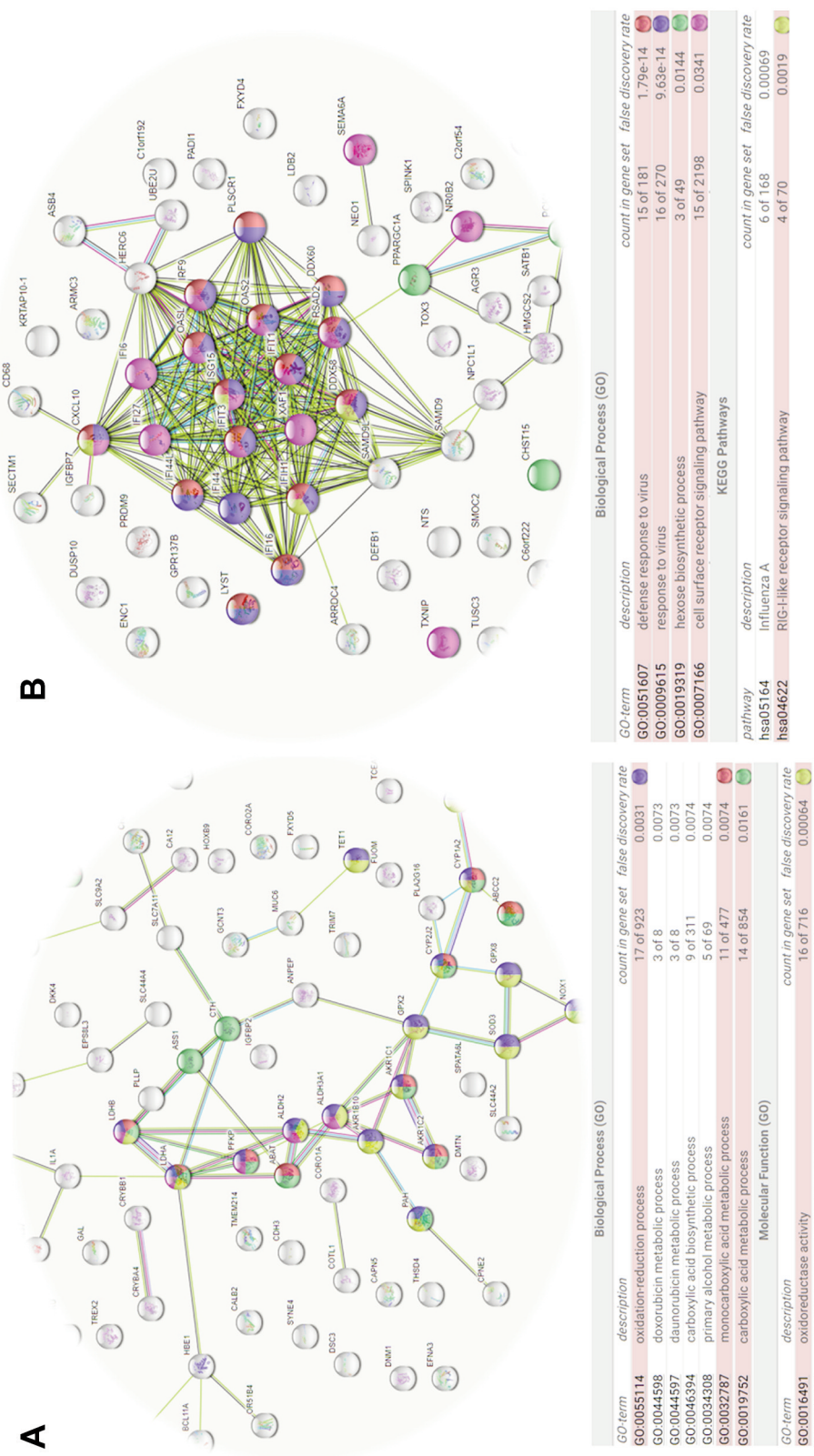

Biological Process (GO)

GO-term	description	count in gene set	false discovery rate
GO:0055114	oxidation-reduction process	17 of 923	0.0031
GO:0044598	doxorubicin metabolic process	3 of 8	0.0073
GO:0044597	daunorubicin metabolic process	3 of 8	0.0073
GO:0046394	carboxylic acid biosynthetic process	9 of 311	0.0074
GO:0034308	primary alcohol metabolic process	5 of 69	0.0074
GO:0032787	monocarboxylic acid metabolic process	11 of 477	0.0074
GO:0019752	carboxylic acid metabolic process	14 of 854	0.0161

Molecular Function (GO)

GO-term	description	count in gene set	false discovery rate
GO:0016491	oxidoreductase activity	16 of 716	0.00064
GO:0004033	aldo-keto reductase (NADP) activity	4 of 25	0.0035
GO:0016620	oxidoreductase activity, acting on the aldehyde or oxo grou...	4 of 31	0.0050
GO:0048037	cofactor binding	11 of 481	0.0056
GO:0016616	oxidoreductase activity, acting on the CH-OH group of dono...	6 of 118	0.0056

KEGG Pathways

pathway	description	count in gene set	false discovery rate
hsa00010	Glycolysis / Gluconeogenesis	5 of 68	0.0050
hsa00590	Arachidonic acid metabolism	4 of 61	0.0232
hsa01230	Biosynthesis of amino acids	4 of 72	0.0253
hsa01100	Metabolic pathways	16 of 1250	0.0253
hsa00640	Propanoate metabolism	3 of 32	0.0253

Biological Process (GO)

GO-term	description	count in gene set	false discovery rate
GO:0051607	defense response to virus	15 of 181	1.79e-14
GO:0009615	response to virus	16 of 270	9.63e-14
GO:0019319	hexose biosynthetic process	3 of 49	0.0144
GO:0007166	cell surface receptor signaling pathway	15 of 2198	0.0341

KEGG Pathways

pathway	description	count in gene set	false discovery rate
hsa05164	Influenza A	6 of 168	0.00069
hsa04622	RIG-I-like receptor signaling pathway	4 of 70	0.0019

Figure 7. *Continued*

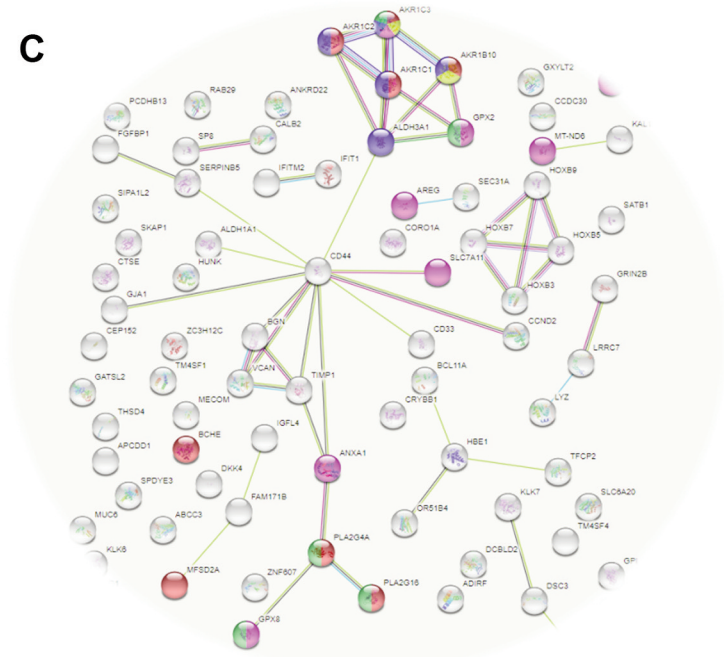

Biological Process (GO)			
GO-term	*description*	*count in gene set*	*false discovery rate*
GO:0044598	doxorubicin metabolic process	4 of 8	0.00024
GO:0044597	daunorubicin metabolic process	4 of 8	0.00024
GO:0097164	ammonium ion metabolic process	8 of 179	0.00031
GO:0016488	farnesol catabolic process	2 of 2	0.0098
GO:0006979	response to oxidative stress	8 of 373	0.0113
Molecular Function (GO)			
GO-term	*description*	*count in gene set*	*false discovery rate*
GO:0004033	aldo-keto reductase (NADP) activity	5 of 25	4.98e-05
GO:0047718	indanol dehydrogenase activity	3 of 3	0.00023
GO:0047115	trans-1,2-dihydrobenzene-1,2-diol dehydrogenase activity	3 of 4	0.00023
GO:0047086	ketosteroid monooxygenase activity	3 of 3	0.00023
KEGG Pathways			
pathway	*description*	*count in gene set*	*false discovery rate*
hsa00590	Arachidonic acid metabolism	5 of 61	0.00080

Biological Process (GO)			
GO-term	*description*	*count in gene set*	*false discovery rate*
GO:0097067	cellular response to thyroid hormone stimulus	3 of 16	0.0275
GO:0071456	cellular response to hypoxia	7 of 139	0.0275
GO:0055114	oxidation-reduction process	16 of 923	0.0275
GO:0019318	hexose metabolic process	6 of 154	0.0414
Molecular Function (GO)			
GO-term	*description*	*count in gene set*	*false discovery rate*
GO:0031418	L-ascorbic acid binding	4 of 20	0.0052
GO:0048029	monosaccharide binding	5 of 66	0.0147
GO:0051213	dioxygenase activity	5 of 88	0.0286
KEGG Pathways			
pathway	*description*	*count in gene set*	*false discovery rate*
hsa04066	HIF-1 signaling pathway	7 of 98	0.00040

Figure 7. *String predicted protein-protein interactions assembled from microarray data specific to DEG down-regulated genes in the LDHA/B DKO clone set, (relative to WT controls). (A) The network nodes connected by a line represent protein-protein interactions, with colored nodes correspond to the String DB functional, molecular or pathway elements in the Table below. The interactions include direct (physical) and indirect (functional) associations; stemming from computational prediction, and knowledge of interactions aggregated from a large number of major (primary) databases. (B) The network nodes connected by a line represent protein-protein interactions, with colored nodes correspond to the String DB functional, molecular or pathway elements in the Table below. The interactions include direct (physical) and indirect (functional) associations; stemming from computational prediction, and knowledge of interactions aggregated from a large number of major (primary) databases. (C) The network nodes connected by a line represent protein-protein interactions, with colored nodes correspond to the String DB functional, molecular or pathway elements in the Table below. The interactions include direct (physical) and indirect (functional) associations; stemming from computational prediction, and knowledge of interactions aggregated from a large number of major (primary) databases. (D) The network nodes connected by a line represent protein-protein interactions, with colored nodes correspond to the String DB functional, molecular or pathway elements in the Table below. The interactions include direct (physical) and indirect (functional) associations; stemming from computational prediction, and knowledge of interactions aggregated from a large number of major (primary) databases.*

Acknowledgements

This research was supported by the National Institute of Minority Health and Health Disparities of the National Institutes of Health through Grant Number G12 MD007582 and Grant Number P20 MD006738 - (Dr J. Pouyssegur's group) Research was funded by University Côte d'Azur, IRCAN, CNRS and by the Centre Scientifique de Monaco and Donation from GEMLUC.

References

1 Kroemer G and Pouyssegur J: Tumor cell metabolism: Cancer's achilles' heel. Cancer Cell *13(6)*: 472-482, 2008. PMID: 18538731. DOI: 10.1016/j.ccr.2008.05.005

2 Cassim S, Vucetic M, Zdralevic M and Pouyssegur J: Warburg and beyond: The power of mitochondrial metabolism to collaborate or replace fermentative glycolysis in cancer. Cancers (Basel) *12(5)*, 2020. PMID: 32365833. DOI: 10.3390/cancers 12051119

3 Pillai SR, Damaghi M, Marunaka Y, Spugnini EP, Fais S and Gillies RJ: Causes, consequences, and therapy of tumors acidosis. Cancer Metastasis Rev *38(1-2)*: 205-222, 2019. PMID: 30911978. DOI: 10.1007/s10555-019-09792-7

4 da Silva VP, Mesquita CB, Nunes JS, de Bem Prunes B, Rados PV and Visioli F: Effects of extracellular acidity on resistance to chemotherapy treatment: A systematic review. Med Oncol *35(12)*: 161, 2018. PMID: 30377828. DOI: 10.1007/s12032-018-1214-4

5 Taddei ML, Pietrovito L, Leo A and Chiarugi P: Lactate in sarcoma microenvironment: Much more than just a waste product. Cells *9(2)*, 2020. PMID: 32102348. DOI: 10.3390/cells9020510

6 Parks SK, Mueller-Klieser W and Pouyssegur J: Lactate and acidity in the cancer microenvironment. Annu Rev Cancer Biol *4*: 141-158, 2020. DOI: 10.1146/annurev-cancerbio-030419- 033556

7 Cassim S and Pouyssegur J: Tumor microenvironment: A metabolic player that shapes the immune response. Int J Mol Sci *21(1)*, 2019. PMID: 31881671. DOI: 10.3390/ijms21010157

8 Chiche J, Brahimi-Horn MC and Pouyssegur J: Tumour hypoxia induces a metabolic shift causing acidosis: A common feature in cancer. J Cell Mol Med *14(4)*: 771-794, 2010. PMID: 20015196. DOI: 10.1111/j.1582-4934.2009.00994.x

9 de la Cruz-Lopez KG, Castro-Munoz LJ, Reyes-Hernandez DO, Garcia-Carranca A and Manzo-Merino J: Lactate in the regulation of tumor microenvironment and therapeutic approaches. Front Oncol *9:* 1143, 2019. PMID: 31737570. DOI: 10.3389/fonc.2019. 01143

10 Wei D, Engelman DM, Reshetnyak YK and Andreev OA: Mapping ph at cancer cell surfaces. Mol Imaging Biol *21(6)*: 1020-1025, 2019. PMID: 30989440. DOI: 10.1007/s11307-019-01335-4

11 Wehr J, Sikorski EL, Bloch E, Feigman MS, Ferraro NJ, Baybutt TR, Snook AE, Pires MM and Thevenin D: Ph-dependent grafting of cancer cells with antigenic epitopes promotes selective antibody-mediated cytotoxicity. J Med Chem *63(7)*: 3713-3722, 2020. PMID: 32196345. DOI: 10.1021/acs.jmedchem.0c00016

12 Schuerle S, Furubayashi M, Soleimany AP, Gwisai T, Huang W, Voigt C and Bhatia SN: Genetic encoding of targeted magnetic resonance imaging contrast agents for tumor imaging. ACS Synth Biol *9(2)*: 392-401, 2020. PMID: 31922737. DOI: 10.1021/acssynbio.9b00416

13 Marchiq I and Pouyssegur J: Hypoxia, cancer metabolism and the therapeutic benefit of targeting lactate/h(+) symporters. J Mol Med (Berl) *94(2)*: 155-171, 2016. PMID: 26099350. DOI: 10.1007/s00109-015-1307-x

14 Deiab S, Mazzio E, Messeha S, Mack N and Soliman KF: High-throughput screening to identify plant derived human ldh-a inhibitors. European J Med Plants *3(4)*: 603-615, 2013. PMID: 24478981. DOI: 10.9734/ejmp/2013/5995

15 Deiab S, Mazzio E, Eyunni S, McTier O, Mateeva N, Elshami F and Soliman KF: 1,2,3,4,6-penta-o-galloylglucose within galla chinensis inhibits human ldh-a and attenuates cell proliferation in mda-mb-231 breast cancer cells. Evid Based Complement Alternat Med *2015:* 276946, 2015. PMID: 25918543. DOI: 10.1155/2015/276946

16 Mack N, Mazzio EA, Bauer D, Flores-Rozas H and Soliman KF: Stable shrna silencing of lactate dehydrogenase a (ldha) in human mda-mb-231 breast cancer cells fails to alter lactic acid production, glycolytic activity, atp or survival. Anticancer Res *37(3)*: 1205-1212, 2017. PMID: 28314283. DOI: 10.21873/anticanres.11435

17 Zdralevic M, Brand A, Di Ianni L, Dettmer K, Reinders J, Singer K, Peter K, Schnell A, Bruss C, Decking SM, Koehl G, Felipe-Abrio B, Durivault J, Bayer P, Evangelista M, O'Brien T, Oefner PJ, Renner K, Pouyssegur J and Kreutz M: Double genetic disruption of lactate dehydrogenases a and b is required to ablate the "warburg effect" restricting tumor growth to oxidative metabolism. J Biol Chem *293(41)*: 15947-15961, 2018. PMID: 30158244. DOI: 10.1074/jbc.RA118.004180

18 de Padua MC, Delodi G, Vucetic M, Durivault J, Vial V, Bayer P, Noleto GR, Mazure NM, Zdralevic M and Pouyssegur J: Disrupting glucose-6-phosphate isomerase fully suppresses the "warburg effect" and activates oxphos with minimal impact on tumor growth except in hypoxia. Oncotarget *8(50)*: 87623-87637, 2017. PMID: 29152106. DOI: 10.18632/oncotarget.21007

19 Zdralevic M, Vucetic M, Daher B, Marchiq I, Parks SK and Pouyssegur J: Disrupting the 'warburg effect' re-routes cancer cells to oxphos offering a vulnerability point *via* 'ferroptosis'-induced cell death. Adv Biol Regul *68:* 55-63, 2018. PMID: 29306548. DOI: 10.1016/j.jbior.2017.12.002

20 Zdralevic M, Marchiq I, de Padua MMC, Parks SK and Pouyssegur J: Metabolic plasiticy in cancers-distinct role of glycolytic enzymes gpi, ldhs or membrane transporters mcts. Front Oncol *7:* 313, 2017. PMID: 29326883. DOI: 10.3389/fonc. 2017.00313

21 Magnani E and Bettini E: Resazurin detection of energy metabolism changes in serum-starved pc12 cells and of neuroprotective agent effect. Brain Res Brain Res Protoc *5(3)*: 266-272, 2000. PMID: 10906492. DOI: 10.1016/s1385-299x(00)00022-2

22 Szklarczyk D, Gable AL, Lyon D, Junge A, Wyder S, Huerta-Cepas J, Simonovic M, Doncheva NT, Morris JH, Bork P, Jensen LJ and Mering CV: String v11: Protein-protein association networks with increased coverage, supporting functional discovery in genome-wide experimental datasets. Nucleic Acids Res *47(D1)*: D607-D613, 2019. PMID: 30476243. DOI: 10.1093/nar/gky1131

23 Szklarczyk D, Morris JH, Cook H, Kuhn M, Wyder S, Simonovic M, Santos A, Doncheva NT, Roth A, Bork P, Jensen LJ and von Mering C: The string database in 2017: Quality-controlled protein-protein association networks, made broadly accessible. Nucleic Acids Res *45(D1)*: D362-D368, 2017. PMID: 27924014. DOI: 10.1093/nar/gkw937

24 Grabacka M, Pierzchalska M, Dean M and Reiss K: Regulation of ketone body metabolism and the role of pparalpha. Int J Mol Sci *17(12)*, 2016. PMID: 27983603. DOI: 10.3390/ijms17122093

25 Liang H and Ward WF: Pgc-1alpha: A key regulator of energy metabolism. Adv Physiol Educ *30(4)*: 145-151, 2006. PMID: 17108241. DOI: 10.1152/advan.00052.2006

26 Cassim S, Raymond VA, Dehbidi-Assadzadeh L, Lapierre P and Bilodeau M: Metabolic reprogramming enables hepatocarcinoma cells to efficiently adapt and survive to a nutrient-restricted microenvironment. Cell Cycle *17(7)*: 903-916, 2018. PMID: 29633904. DOI: 10.1080/15384101.2018.1460023

27 Lacoste B, Raymond VA, Cassim S, Lapierre P and Bilodeau M: Highly tumorigenic hepatocellular carcinoma cell line with cancer stem cell-like properties. PLoS One *12(2)*: e0171215, 2017. PMID: 28152020. DOI: 10.1371/journal.pone.0171215

28 Song JP, Chen L, Chen X, Ren J, Zhang NN, Tirasawasdichai T, Hu ZL, Hua W, Hu YR, Tang HR, Chen HV and Hu SS: Elevated plasma beta-hydroxybutyrate predicts adverse outcomes and disease progression in patients with arrhythmogenic cardiomyopathy. Sci Transl Med *12(530)*: eaay8329, 2020. PMID: 32051229. DOI: 10.1126/scitranslmed.aay8329

29 Kim JT, Li C, Weiss HL, Zhou Y, Liu C, Wang Q and Evers BM: Regulation of ketogenic enzyme hmgcs2 by wnt/beta-catenin/ppargamma pathway in intestinal cells. Cells *8(9)*, 2019. PMID: 31546785. DOI: 10.3390/cells8091106

30 Gharib E, Nasrinasrabadi P and Zali MR: Development and validation of a lipogenic genes panel for diagnosis and recurrence of colorectal cancer. PLoS One *15(3)*: e0229864, 2020. PMID: 32155177. DOI: 10.1371/journal.pone.0229864

31 Low END, Mokhtar NM, Wong Z and Raja Ali RA: Colonic mucosal transcriptomic changes in patients with long-duration ulcerative colitis revealed colitis-associated cancer pathways. J Crohns Colitis *13(6)*: 755-763, 2019. PMID: 30954025. DOI: 10.1093/ecco-jcc/jjz002

32 Hu D, Zhou M and Zhu X: Deciphering immune-associated genes to predict survival in clear cell renal cell cancer. Biomed Res Int *2019:* 2506843, 2019. PMID: 31886185. DOI: 10.1155/2019/2506843

33 Xu WH, Xu Y, Wang J, Wan FN, Wang HK, Cao DL, Shi GH, Qu YY, Zhang HL and Ye DW: Prognostic value and immune infiltration of novel signatures in clear cell renal cell carcinoma microenvironment. Aging (Albany NY) *11(17)*: 6999-7020, 2019. PMID: 31493764. DOI: 10.18632/aging.102233

34 Li N, Li H, Cao L and Zhan X: Quantitative analysis of the mitochondrial proteome in human ovarian carcinomas. Endocr Relat Cancer *25(10)*: 909-931, 2018. PMID: 29997262. DOI: 10.1530/ERC-18-0243

35 Su SG, Yang M, Zhang MF, Peng QZ, Li MY, Liu LP and Bao SY: Mir-107-mediated decrease of hmgcs2 indicates poor outcomes and promotes cell migration in hepatocellular carcinoma. Int J Biochem Cell Biol *91(Pt A)*: 53-59, 2017. PMID: 28867541. DOI: 10.1016/j.biocel.2017.08.016

36 Chen SW, Chou CT, Chang CC, Li YJ, Chen ST, Lin IC, Kok SH, Cheng SJ, Lee JJ, Wu TS, Kuo ML and Lin BR: Hmgcs2 enhances invasion and metastasis *via* direct interaction with pparalpha to activate src signaling in colorectal cancer and oral cancer. Oncotarget *8(14)*: 22460-22476, 2017. PMID: 27816970. DOI: 10.18632/oncotarget.13006

37 Saraon P, Cretu D, Musrap N, Karagiannis GS, Batruch I, Drabovich AP, van der Kwast T, Mizokami A, Morrissey C, Jarvi K and Diamandis EP: Quantitative proteomics reveals that enzymes of the ketogenic pathway are associated with prostate cancer progression. Mol Cell Proteomics *12(6)*: 1589-1601, 2013. PMID: 23443136. DOI: 10.1074/mcp.M112.023887

38 Kumamoto K, Nakachi Y, Mizuno Y, Yokoyama M, Ishibashi K, Kosugi C, Koda K, Kobayashi M, Tanakaya K, Matsunami T, Eguchi H, Okazaki Y and Ishida H: Expressions of 10 genes as candidate predictors of recurrence in stage III colon cancer patients receiving adjuvant oxaliplatin-based chemotherapy. Oncol Lett *18(2)*: 1388-1394, 2019. PMID: 31423202. DOI: 10.3892/ol.2019.10437

39 Martinez-Outschoorn UE, Lin Z, Whitaker-Menezes D, Howell A, Sotgia F and Lisanti MP: Ketone body utilization drives tumor growth and metastasis. Cell Cycle *11(21)*: 3964-3971, 2012. PMID: 23082722. DOI: 10.4161/cc.22137

40 Hu J and Yu Y: The function of thioredoxin-binding protein-2 (tbp-2) in different diseases. Oxid Med Cell Longev *2018:* 4582130, 2018. PMID: 29854083. DOI: 10.1155/2018/4582130

41 Tang G, Duan F, Li W, Wang Y, Zeng C, Hu J, Li H, Zhang X, Chen Y and Tan H: Metformin inhibited nod-like receptor protein 3 inflammasomes activation and suppressed diabetes-accelerated atherosclerosis in apoe(–/–) mice. Biomed Pharmacother *119:* 109410, 2019. PMID: 31518877. DOI: 10.1016/j.biopha.2019.109410

42 Pouyssegur J, Franchi A, Salomon JC and Silvestre P: Isolation of a Chinese hamster fibroblast mutant defective in hexose transport and aerobic glycolysis: Its use to dissect the malignant phenotype. Proc Natl Acad Sci USA *77(5)*: 2698-2701, 1980. PMID: 6930659. DOI: 10.1073/pnas.77.5.2698

43 Stoltzman CA, Kaadige MR, Peterson CW and Ayer DE: Mondoa senses non-glucose sugars: Regulation of thioredoxin-interacting protein (txnip) and the hexose transport curb. J Biol Chem *286(44)*: 38027-38034, 2011. PMID: 21908621. DOI: 10.1074/jbc.M111.275503

44 Wu N, Zheng B, Shaywitz A, Dagon Y, Tower C, Bellinger G, Shen CH, Wen J, Asara J, McGraw TE, Kahn BB and Cantley LC: Ampk-dependent degradation of txnip upon energy stress leads to enhanced glucose uptake *via* glut1. Mol Cell *49(6)*: 1167-1175, 2013. PMID: 23453806. DOI: 10.1016/j.molcel.2013.01.035

45 Jiang X, Pang Y, Zhao S, Hao H, Zhao X, Du W, Wang Y and Zhu H: Thioredoxin-interacting protein regulates glucose metabolism and improves the intracellular redox state in bovine oocytes during *in vitro* maturation. Am J Physiol Endocrinol Metab *318(3)*: E405-E416, 2020. PMID: 31935112. DOI: 10.1152/ajpendo.00057.2019

46 Qu X, Sun J, Zhang Y, Li J, Hu J, Li K, Gao L and Shen L: C-myc-driven glycolysis *via* txnip suppression is dependent on glutaminase-mondoa axis in prostate cancer. Biochem Biophys Res Commun *504(2)*: 415-421, 2018. PMID: 30103944. DOI: 10.1016/j.bbrc.2018.08.069

47 Shen L, O'Shea JM, Kaadige MR, Cunha S, Wilde BR, Cohen AL, Welm AL and Ayer DE: Metabolic reprogramming in triple-negative breast cancer through myc suppression of txnip. Proc Natl Acad Sci USA *112(17)*: 5425-5430, 2015. PMID: 25870263. DOI: 10.1073/pnas.1501555112

48 Vassalli G: Aldehyde dehydrogenases: Not just markers, but functional regulators of stem cells. Stem Cells Int *2019:* 3904645, 2019. PMID: 30733805. DOI: 10.1155/2019/3904645

49 Zhong G, Kirkwood J, Won KJ, Tjota N, Jeong H and Isoherranen N: Characterization of vitamin a metabolome in human livers with and without nonalcoholic fatty liver disease. J Pharmacol Exp Ther *370(1)*: 92-103, 2019. PMID: 31043436. DOI: 10.1124/jpet.119.258517

50 Wang Y, Wang CH, Zhang YF, Zhu L, Lei HM and Tang YB: Uplc-ms-based metabolomics reveals metabolic dysregulation in aldh1a1-overexpressed lung adenocarcinoma cells. Metabolomics *15(4)*: 52, 2019. PMID: 30911937. DOI: 10.1007/s11306-019-1514-5

51 Calleja LF, Belmont-Diaz JA, Medina-Contreras O, Quezada H, Yoval-Sanchez B, Campos-Garcia J and Rodriguez-Zavala JS: Omeprazole as a potent activator of human cytosolic aldehyde dehydrogenase aldh1a1. Biochim Biophys Acta Gen Subj *1864(1)*: 129451, 2020. PMID: 31678145. DOI: 10.1016/j.bbagen.2019.129451

52 Fei X, Wang G, Shen H and Gu X: Placenta-specific 8 is a potential novel target for osimertinib resistance in non-small cell lung cancer. Oncol Lett *18(1)*: 955-961, 2019. PMID: 31289574. DOI: 10.3892/ol.2019.10344

53 McKinney A, Lindberg OR, Engler JR, Chen KY, Kumar A, Gong H, Lu KV, Simonds EF, Cloughesy TF, Liau LM, Prados M, Bollen AW, Berger MS, Shieh JTC, James CD, Nicolaides TP, Yong WH, Lai A, Hegi ME, Weiss WA and Phillips JJ: Mechanisms of resistance to egfr inhibition reveal metabolic vulnerabilities in human gbm. Mol Cancer Ther *18(9)*: 1565-1576, 2019. PMID: 31270152. DOI: 10.1158/1535-7163.MCT-18-1330

54 Li L, Wang Y, Jiao L, Lin C, Lu C, Zhang K, Hu C, Ye J, Zhang D, Wu H, Feng M and He Y: Protective autophagy decreases osimertinib cytotoxicity through regulation of stem cell-like properties in lung cancer. Cancer Lett *452:* 191-202, 2019. PMID: 30910592. DOI: 10.1016/j.canlet.2019.03.027

55 Osmanov YI, Kogan EA, Rapoport LM, Teodorovich OV and Gaibov JA: [Markers of stem cells and their prognostic values for urothelial carcinomas of the urinary tract]. Urologiia *(2)*: 40-49, 2019. PMID: 31162900.

56 Kim HM and Koo JS: Immunohistochemical analysis of cancer stem cell marker expression in papillary thyroid cancer. Front Endocrinol (Lausanne) *10:* 523, 2019. PMID: 31428052. DOI: 10.3389/fendo.2019.00523

57 Elcheva IA, Wood T, Chiarolanzio K, Chim B, Wong M, Singh V, Gowda CP, Lu Q, Hafner M, Dovat S, Liu Z, Muljo SA and Spiegelman VS: Rna-binding protein igf2bp1 maintains leukemia stem cell properties by regulating hoxb4, myb, and aldh1a1. Leukemia, 2019. PMID: 31768017. DOI: 10.1038/s41375-019-0656-9

58 Qin B, Zou S, Li K, Wang H, Wei W, Zhang B, Xiao L, Choi HH, Tang Q, Huang D, Liu Q, Pan Q, Meng M, Fang L and Lee MH: Csn6-trim21 axis instigates cancer stemness during tumorigenesis. Br J Cancer, 2020. PMID: 32225170. DOI: 10.1038/s41416-020-0779-9

59 Tsunedomi R, Yoshimura K, Suzuki N, Hazama S and Nagano H: Clinical implications of cancer stem cells in digestive cancers: Acquisition of stemness and prognostic impact. Surg Today, 2020. PMID: 32025858. DOI: 10.1007/s00595-020-01968-x

60 Rebollido-Rios R, Venton G, Sanchez-Redondo S, Iglesias IFC, Fournet G, Gonzalez E, Romero Fernandez W, Borroto Escuela DO, Di Stefano B, Penarroche-Diaz R, Martin G, Ceylan I, Costello R and Perez-Alea M: Dual disruption of aldehyde dehydrogenases 1 and 3 promotes functional changes in the glutathione redox system and enhances chemosensitivity in nonsmall cell lung cancer. Oncogene *39(13)*: 2756-2771, 2020. PMID: 32015486. DOI: 10.1038/s41388-020-1184-9

61 Liu WT, Liu WB, Gao M, Zhang YY and Gu KS: Expression of aldh1a1 and cd133 is associated with the prognosis and effect of different chemotherapeutic regimens in gastric cancer. Oncol Lett *18(5)*: 4573-4582, 2019. PMID: 31611965. DOI: 10.3892/ol.2019.10798

62 Liang D, Fan Y, Yang Z, Zhang Z, Liu M, Liu L and Jiang C: Discovery of coumarin-based selective aldehyde dehydrogenase 1a1 inhibitors with glucose metabolism improving activity. Eur J Med Chem *187:* 111923, 2020. PMID: 31816557. DOI: 10.1016/j.ejmech.2019.111923

63 Hu Z, Wu J, Qin L, Jin H, Lv Y, Zhang R, Xiao C, Cao Y and Zhao Y: Aldh1a1 effect on yan yellow cattle preadipocyte differentiation. Anim Biotechnol: 1-10, 2019. PMID: 31646946. DOI: 10.1080/10495398.2019.1679824

64 Mori Y, Yamawaki K, Ishiguro T, Yoshihara K, Ueda H, Sato A, Ohata H, Yoshida Y, Minamino T, Okamoto K and Enomoto T: Aldh-dependent glycolytic activation mediates stemness and paclitaxel resistance in patient-derived spheroid models of uterine endometrial cancer. Stem Cell Reports *13(4)*: 730-746, 2019. PMID: 31564647. DOI: 10.1016/j.stemcr.2019.08.015

65 Namiki K, Wongsirisin P, Yokoyama S, Sato M, Rawangkan A, Sakai R, Iida K and Suganuma M: (-)-epigallocatechin gallate inhibits stemness and tumourigenicity stimulated by axl receptor tyrosine kinase in human lung cancer cells. Sci Rep *10(1)*: 2444, 2020. PMID: 32051483. DOI: 10.1038/s41598-020-59281-z

66 Sun X, Song J, Li E, Geng H, Li Y, Yu D and Zhong C: ()epigallocatechin3gallate inhibits bladder cancer stem cells *via* suppression of sonic hedgehog pathway. Oncol Rep *42(1)*: 425-435, 2019. PMID: 31180522. DOI: 10.3892/or.2019.7170

67 Sridharan S, Robeson M, Bastihalli-Tukaramrao D, Howard CM, Subramaniyan B, Tilley AMC, Tiwari AK and Raman D: Targeting of the eukaryotic translation initiation factor 4a against breast cancer stemness. Front Oncol *9:* 1311, 2019. PMID: 31867270. DOI: 10.3389/fonc.2019.01311

68 Wang L, Wei Y, Ning C, Zhang M, Fan P, Lei D, Du J, Gale M, Ma Y and Yang Y: Ellagic acid promotes browning of white adipose tissues in high-fat diet-induced obesity in rats through suppressing white adipocyte maintaining genes. Endocr J *66(10)*: 923-936, 2019. PMID: 31292308. DOI: 10.1507/endocrj.EJ18-0467

69 Matsunaga T, Morikawa Y, Haga M, Endo S, Soda M, Yamamura K, El-Kabbani O, Tajima K, Ikari A and Hara A: Exposure to 9,10-phenanthrenequinone accelerates malignant progression of lung cancer cells through up-regulation of aldo-keto reductase 1b10. Toxicol Appl Pharmacol *278(2)*: 180-189, 2014. PMID: 24813866. DOI: 10.1016/j.taap.2014.04.024

70 Sato S, Genda T, Ichida T, Murata A, Tsuzura H, Narita Y, Kanemitsu Y, Ishikawa S, Kikuchi T, Mori M, Hirano K, Iijima K, Wada R, Nagahara A and Watanabe S: Impact of aldo-keto reductase family 1 member b10 on the risk of hepatitis c virus-related hepatocellular carcinoma. J Gastroenterol Hepatol *31(7)*: 1315-1322, 2016. PMID: 26758591. DOI: 10.1111/jgh.13295

71 Mori M, Genda T, Ichida T, Murata A, Kamei M, Tsuzura H, Sato S, Narita Y, Kanemitsu Y, Ishikawa S, Kikuchi T, Shimada Y, Hirano K, Iijima K, Sugimoto K, Wada R, Nagahara A and Watanabe S: Aldo-keto reductase family 1 member b10 is associated with hepatitis b virus-related hepatocellular carcinoma

risk. Hepatol Res *47(3)*: E85-E93, 2017. PMID: 27084455. DOI: 10.1111/hepr.12725

72 Qi LN, Li LQ, Chen YY, Chen ZH, Bai T, Xiang BD, Qin X, Xiao KY, Peng MH, Liu ZM, Liu TW, Qin X, Li S, Han ZG, Mo ZN, Santella RM, Winkler CA, O'Brien SJ and Peng T: Genome-wide and differential proteomic analysis of hepatitis b virus and aflatoxin b1 related hepatocellular carcinoma in guangxi, china. PLoS One *8(12)*: e83465, 2013. PMID: 24391771. DOI: 10.1371/journal.pone.0083465

73 Feng G, Li XP, Niu CY, Liu ML, Yan QQ, Fan LP, Li Y, Zhang KL, Gao J, Qian MR, He N and Mi M: Bioinformatics analysis reveals novel core genes associated with nonalcoholic fatty liver disease and nonalcoholic steatohepatitis. Gene *742:* 144549, 2020. PMID: 32184169. DOI: 10.1016/j.gene.2020.144549

74 Kanno M, Kawaguchi K, Honda M, Horii R, Takatori H, Shimakami T, Kitamura K, Arai K, Yamashita T, Sakai Y, Yamashita T, Mizukoshi E and Kaneko S: Serum aldo-keto reductase family 1 member b10 predicts advanced liver fibrosis and fatal complications of nonalcoholic steatohepatitis. J Gastroenterol *54(6)*: 549-557, 2019. PMID: 30707282. DOI: 10.1007/s00535-019-01551-3

75 Shi J, Chen L, Chen Y, Lu Y, Chen X and Yang Z: Aldo-keto reductase family 1 member b10 (akr1b10) overexpression in tumors predicts worse overall survival in hepatocellular carcinoma. J Cancer *10(20)*: 4892-4901, 2019. PMID: 31598161. DOI: 10.7150/jca.32768

76 Huang L, He R, Luo W, Zhu YS, Li J, Tan T, Zhang X, Hu Z and Luo D: Aldo-keto reductase family 1 member b10 inhibitors: Potential drugs for cancer treatment. Recent Pat Anticancer Drug Discov *11(2)*: 184-196, 2016. PMID: 26844556. DOI: 10.2174/1574892811888160304113346

77 Zhao SF, Wang SG, Zhao ZY and Li WL: Akr1c1-3, notably akr1c3, are distinct biomarkers for liver cancer diagnosis and prognosis: Database mining in malignancies. Oncol Lett *18(5)*: 4515-4522, 2019. PMID: 31611960. DOI: 10.3892/ol.2019.10802

78 Sonohara F, Inokawa Y, Hishida M, Kanda M, Nishikawa Y, Yamada S, Fujii T, Sugimoto H, Kodera Y and Nomoto S: Prognostic significance of akr1b10 gene expression in hepatocellular carcinoma and surrounding non-tumorous liver tissue. Oncol Lett *12(6)*: 4821-4828, 2016. PMID: 28105190. DOI: 10.3892/ol.2016.5240

79 O'Reilly MW, House PJ and Tomlinson JW: Understanding androgen action in adipose tissue. J Steroid Biochem Mol Biol *143:* 277-284, 2014. PMID: 24787657. DOI: 10.1016/j.jsbmb.2014.04.008

80 Weber S, Salabei JK, Moller G, Kremmer E, Bhatnagar A, Adamski J and Barski OA: Aldo-keto reductase 1b15 (akr1b15): A mitochondrial human aldo-keto reductase with activity toward steroids and 3-keto-acyl-coa conjugates. J Biol Chem *290(10)*: 6531-6545, 2015. PMID: 25577493. DOI: 10.1074/jbc.M114.610121

81 Rizner TL and Penning TM: Role of aldo-keto reductase family 1 (akr1) enzymes in human steroid metabolism. Steroids *79:* 49-63, 2014. PMID: 24189185. DOI: 10.1016/j.steroids.2013.10.012

82 Han C, Gao L, Bai H and Dou X: Identification of a role for serum aldo-keto reductase family 1 member b10 in early detection of hepatocellular carcinoma. Oncol Lett *16(6)*: 7123-7130, 2018. PMID: 30546447. DOI: 10.3892/ol.2018.9547

83 Hung JJ, Yeh YC and Hsu WH: Prognostic significance of akr1b10 in patients with resected lung adenocarcinoma. Thorac Cancer *9(11)*: 1492-1499, 2018. PMID: 30253058. DOI: 10.1111/1759-7714.12863

84 Han C, Gao L, Zhao L, Sheng Q, Zhang C, An Z, Xia T, Ding Y, Wang J, Bai H and Dou X: Immunohistochemistry detects increased expression of aldo-keto reductase family 1 member b10 (akr1b10) in early-stage hepatocellular carcinoma. Med Sci Monit *24:* 7414-7423, 2018. PMID: 30328412. DOI: 10.12659/MSM.910738

85 DiStefano JK and Davis B: Diagnostic and prognostic potential of akr1b10 in human hepatocellular carcinoma. Cancers (Basel) *11(4)*, 2019. PMID: 30959792. DOI: 10.3390/cancers11040486

86 Seifert M, Peitzsch C, Gorodetska I, Borner C, Klink B and Dubrovska A: Network-based analysis of prostate cancer cell lines reveals novel marker gene candidates associated with radioresistance and patient relapse. PLoS Comput Biol *15(11)*: e1007460, 2019. PMID: 31682594. DOI: 10.1371/journal.pcbi.1007460

87 Fang CY, Lin YH and Chen CL: Overexpression of akr1b10 predicts tumor recurrence and short survival in oral squamous cell carcinoma patients. J Oral Pathol Med *48(8)*: 712-719, 2019. PMID: 31237374. DOI: 10.1111/jop.12891

88 Ko HH, Peng HH, Cheng SJ and Kuo MY: Increased salivary akr1b10 level: Association with progression and poor prognosis of oral squamous cell carcinoma. Head Neck *40(12)*: 2642-2647, 2018. PMID: 30430672. DOI: 10.1002/hed.25370

89 Ko HH, Cheng SL, Lee JJ, Chen HM, Kuo MY and Cheng SJ: Expression of akr1b10 as an independent marker for poor prognosis in human oral squamous cell carcinoma. Head Neck *39(7)*: 1327-1332, 2017. PMID: 28301069. DOI: 10.1002/hed.24759

90 Cheng BY, Lau EY, Leung HW, Leung CO, Ho NP, Gurung S, Cheng LK, Lin CH, Lo RC, Ma S, Ng IO and Lee TK: Irak1 augments cancer stemness and drug resistance *via* the ap-1/akr1b10 signaling cascade in hepatocellular carcinoma. Cancer Res *78(9)*: 2332-2342, 2018. PMID: 29483095. DOI: 10.1158/0008-5472.CAN-17-2445

91 Cubillos-Angulo JM, Fukutani ER, Cruz LAB, Arriaga MB, Lima JV, Andrade BB, Queiroz ATL and Fukutani KF: Systems biology analysis of publicly available transcriptomic data reveals a critical link between akr1b10 gene expression, smoking and occurrence of lung cancer. PLoS One *15(2)*: e0222552, 2020. PMID: 32097409. DOI: 10.1371/journal.pone.0222552

92 Chung YT, Matkowskyj KA, Li H, Bai H, Zhang W, Tsao MS, Liao J and Yang GY: Overexpression and oncogenic function of aldo-keto reductase family 1b10 (akr1b10) in pancreatic carcinoma. Mod Pathol *25(5)*: 758-766, 2012. PMID: 22222635. DOI: 10.1038/modpathol.2011.191

93 Matkowskyj KA, Bai H, Liao J, Zhang W, Li H, Rao S, Omary R and Yang GY: Aldoketoreductase family 1b10 (akr1b10) as a biomarker to distinguish hepatocellular carcinoma from benign liver lesions. Hum Pathol *45(4)*: 834-843, 2014. PMID: 24656094. DOI: 10.1016/j.humpath.2013.12.002

94 Zemanova L, Hofman J, Novotna E, Musilek K, Lundova T, Havrankova J, Hostalkova A, Chlebek J, Cahlikova L and Wsol V: Flavones inhibit the activity of akr1b10, a promising therapeutic target for cancer treatment. J Nat Prod *78(11)*: 2666-2674, 2015. PMID: 26529431. DOI: 10.1021/acs.jnatprod.5b00616

95 Jin YY, Han C, Geng N, Li YR, Zheng LY, Zhu WJ, Li YW, An ZY, Zhao LR, Wang JY, Dou XG and Bai H: [akr1b10 inhibitor

enhances the inhibitory effect of sorafenib on liver cancer xenograft]. Zhonghua Gan Zang Bing Za Zhi *27(1)*: 39-44, 2019. PMID: 30685922. DOI: 10.3760/cma.j.issn.1007-3418.2019.01.009

96 Seliger JM, Cicek SS, Witt LT, Martin HJ, Maser E and Hintzpeter J: Selective inhibition of human akr1b10 by n-humulone, adhumulone and cohumulone isolated from humulus lupulus extract. Molecules *23(11)*, 2018. PMID: 30469331. DOI: 10.3390/molecules23113041

97 Seliger JM, Misuri L, Maser E and Hintzpeter J: The hop-derived compounds xanthohumol, isoxanthohumol and 8-prenylnaringenin are tight-binding inhibitors of human aldo-keto reductases 1b1 and 1b10. J Enzyme Inhib Med Chem *33(1)*: 607-614, 2018. PMID: 29532688. DOI: 10.1080/14756366.2018.1437728

98 Zeng CM, Chang LL, Ying MD, Cao J, He QJ, Zhu H and Yang B: Aldo-keto reductase akr1c1-akr1c4: Functions, regulation, and intervention for anti-cancer therapy. Front Pharmacol *8:* 119, 2017. PMID: 28352233. DOI: 10.3389/fphar.2017.00119

99 Ischenko I, Seeliger H, Schaffer M, Jauch KW and Bruns CJ: Cancer stem cells: How can we target them? Curr Med Chem *15(30)*: 3171-3184, 2008. PMID: 19075661. DOI: 10.2174/092986708786848541

100 Cannon MJ, Ghosh D and Gujja S: Signaling circuits and regulation of immune suppression by ovarian tumor-associated macrophages. Vaccines (Basel) *3(2)*: 448-466, 2015. PMID: 26343197. DOI: 10.3390/vaccines3020448

101 Patel S, Barkell AM, Gupta D, Strong SL, Bruton S, Muskett FW, Addis PW, Renshaw PS, Slocombe PM, Doyle C, Clargo A, Taylor RJ, Prosser CE, Henry AJ, Robinson MK, Waters LC, Holdsworth G and Carr MD: Structural and functional analysis of dickkopf 4 (dkk4): New insights into dkk evolution and regulation of wnt signaling by dkk and kremen proteins. J Biol Chem *293(31)*: 12149-12166, 2018. PMID: 29925589. DOI: 10.1074/jbc.RA118.002918

102 Cruciat CM and Niehrs C: Secreted and transmembrane wnt inhibitors and activators. Cold Spring Harb Perspect Biol *5(3)*: a015081, 2013. PMID: 23085770. DOI: 10.1101/cshperspect.a015081

103 Eshelman MA, Shah M, Raup-Konsavage WM, Rennoll SA and Yochum GS: Tcf7l1 recruits ctbp and hdac1 to repress dickkopf4 gene expression in human colorectal cancer cells. Biochem Biophys Res Commun *487(3)*: 716-722, 2017. PMID: 28450117. DOI: 10.1016/j.bbrc.2017.04.123

104 Shimomura Y, Agalliu D, Vonica A, Luria V, Wajid M, Baumer A, Belli S, Petukhova L, Schinzel A, Brivanlou AH, Barres BA and Christiano AM: Apcdd1 is a novel wnt inhibitor mutated in hereditary hypotrichosis simplex. Nature *464(7291)*: 1043-1047, 2010. PMID: 20393562. DOI: 10.1038/nature08875

105 Mazzoni J, Smith JR, Shahriar S, Cutforth T, Ceja B and Agalliu D: The wnt inhibitor apcdd1 coordinates vascular remodeling and barrier maturation of retinal blood vessels. Neuron *96(5)*: 1055-1069 e1056, 2017. PMID: 29154126. DOI: 10.1016/j.neuron.2017.10.025

106 Cho SG: Apc downregulated 1 inhibits breast cancer cell invasion by inhibiting the canonical wnt signaling pathway. Oncol Lett *14(4)*: 4845-4852, 2017. PMID: 29085490. DOI: 10.3892/ol.2017.6801

107 Ashktorab H, Daremipouran M, Devaney J, Varma S, Rahi H, Lee E, Shokrani B, Schwartz R, Nickerson ML and Brim H: Identification of novel mutations by exome sequencing in african american colorectal cancer patients. Cancer *121(1)*: 34-42, 2015. PMID: 25250560. DOI: 10.1002/cncr.28922

108 Zhai W, Hu GH, Zheng JH, Peng B, Liu M, Huang JH, Wang GC, Yao XD and Xu YF: High expression of the secreted protein dickkopf homolog 4: Roles in invasion and metastasis of renal cell carcinoma and its association with von hippel-lindau gene. Int J Mol Med *33(5)*: 1319-1326, 2014. PMID: 24573574. DOI: 10.3892/ijmm.2014.1673

109 Wang S, Wei H and Zhang S: Dickkopf-4 is frequently overexpressed in epithelial ovarian carcinoma and promotes tumor invasion. BMC Cancer *17(1)*: 455, 2017. PMID: 28666421. DOI: 10.1186/s12885-017-3407-1

110 Wang M, Ni B, Zhuang C, Zhao WY, Tu L, Ma XL, Yang LX, Zhang ZG and Cao H: Aberrant accumulation of dickkopf 4 promotes tumor progression *via* forming the immune suppressive microenvironment in gastrointestinal stromal tumor. Cancer Med *8(11)*: 5352-5366, 2019. PMID: 31353847. DOI: 10.1002/cam4.2437

111 Cai X, Yao Z, Li L and Huang J: Role of dkk4 in tumorigenesis and tumor progression. Int J Biol Sci *14(6)*: 616-621, 2018. PMID: 29904276. DOI: 10.7150/ijbs.24329

112 Pendas-Franco N, Garcia JM, Pena C, Valle N, Palmer HG, Heinaniemi M, Carlberg C, Jimenez B, Bonilla F, Munoz A and Gonzalez-Sancho JM: Dickkopf-4 is induced by tcf/beta-catenin and upregulated in human colon cancer, promotes tumour cell invasion and angiogenesis and is repressed by 1alpha,25-dihydroxyvitamin d3. Oncogene *27(32)*: 4467-4477, 2008. PMID: 18408752. DOI: 10.1038/onc.2008.88

113 Ebert MP, Tanzer M, Balluff B, Burgermeister E, Kretzschmar AK, Hughes DJ, Tetzner R, Lofton-Day C, Rosenberg R, Reinacher-Schick AC, Schulmann K, Tannapfel A, Hofheinz R, Rocken C, Keller G, Langer R, Specht K, Porschen R, Stohlmacher-Williams J, Schuster T, Strobel P and Schmid RM: Tfap2e-dkk4 and chemoresistance in colorectal cancer. N Engl J Med *366(1)*: 44-53, 2012. PMID: 22216841. DOI: 10.1056/NEJMoa1009473

114 He S, Shen J, Hu N, Xu X and Li J: Dkk4 enhances resistance to chemotherapeutics 5-fu and yn968d1 in colorectal cancer cells. Oncol Lett *13(2)*: 587-592, 2017. PMID: 28356933. DOI: 10.3892/ol.2016.5461

115 Chen HJ, Sun J, Huang Z, Hou H, Jr., Arcilla M, Rakhilin N, Joe DJ, Choi J, Gadamsetty P, Milsom J, Nandakumar G, Longman R, Zhou XK, Edwards R, Chen J, Chen KY, Bu P, Wang L, Xu Y, Munroe R, Abratte C, Miller AD, Gumus ZH, Shuler M, Nishimura N, Edelmann W, Shen X and Lipkin SM: Comprehensive models of human primary and metastatic colorectal tumors in immunodeficient and immunocompetent mice by chemokine targeting. Nat Biotechnol *33(6)*: 656-660, 2015. PMID: 26006007. DOI: 10.1038/nbt.3239

116 Zeng S, Seifert AM, Zhang JQ, Cavnar MJ, Kim TS, Balachandran VP, Santamaria-Barria JA, Cohen NA, Beckman MJ, Medina BD, Rossi F, Crawley MH, Loo JK, Maltbaek JH, Besmer P, Antonescu CR and DeMatteo RP: Wnt/beta-catenin signaling contributes to tumor malignancy and is targetable in gastrointestinal stromal tumor. Mol Cancer Ther *16(9)*: 1954-1966, 2017. PMID: 28611108. DOI: 10.1158/1535-7163.MCT-17-0139

117 Chouhan S, Singh S, Athavale D, Ramteke P, Pandey V, Joseph J, Mohan R, Shetty PK and Bhat MK: Glucose induced activation of canonical wnt signaling pathway in hepatocellular carcinoma is regulated by dkk4. Sci Rep *6:* 27558, 2016. PMID: 27272409. DOI: 10.1038/srep27558

118 Hirata H, Hinoda Y, Majid S, Chen Y, Zaman MS, Ueno K, Nakajima K, Tabatabai ZL, Ishii N and Dahiya R: Dickkopf-4 activates the noncanonical c-jun-nh2 kinase signaling pathway while inhibiting the wnt-canonical pathway in human renal cell carcinoma. Cancer *117(8)*: 1649-1660, 2011. PMID: 21472712. DOI: 10.1002/cncr.25666

119 Chau WK, Ip CK, Mak AS, Lai HC and Wong AS: C-kit mediates chemoresistance and tumor-initiating capacity of ovarian cancer cells through activation of wnt/beta-catenin-atp-binding cassette g2 signaling. Oncogene *32(22)*: 2767-2781, 2013. PMID: 22797058. DOI: 10.1038/onc.2012.290

120 Dakhova O, Rowley D and Ittmann M: Genes upregulated in prostate cancer reactive stroma promote prostate cancer progression *in vivo*. Clin Cancer Res *20(1)*: 100-109, 2014. PMID: 24150235. DOI: 10.1158/1078-0432.CCR-13-1184

121 Humbert M, Casteran N, Letard S, Hanssens K, Iovanna J, Finetti P, Bertucci F, Bader T, Mansfield CD, Moussy A, Hermine O and Dubreuil P: Masitinib combined with standard gemcitabine chemotherapy: *In vitro* and *in vivo* studies in human pancreatic tumour cell lines and ectopic mouse model. PLoS One *5(3)*: e9430, 2010. PMID: 20209107. DOI: 10.1371/journal.pone.0009430

122 Gu X, Ma Y, Xiao J, Zheng H, Song C, Gong Y and Xing X: Up-regulated biglycan expression correlates with the malignancy in human colorectal cancers. Clin Exp Med *12(3)*: 195-199, 2012. PMID: 21879307. DOI: 10.1007/s10238-011-0155-4

123 Guo D, Zhang W, Yang H, Bi J, Xie Y, Cheng B, Wang Y and Chen S: Celastrol induces necroptosis and ameliorates inflammation *via* targeting biglycan in human gastric carcinoma. Int J Mol Sci *20(22)*, 2019. PMID: 31739592. DOI: 10.3390/ijms20225716

124 Hu L, Duan YT, Li JF, Su LP, Yan M, Zhu ZG, Liu BY and Yang QM: Biglycan enhances gastric cancer invasion by activating fak signaling pathway. Oncotarget *5(7)*: 1885-1896, 2014. PMID: 24681892. DOI: 10.18632/oncotarget.1871

125 Xing X, Gu X and Ma T: Knockdown of biglycan expression by RNA interference inhibits the proliferation and invasion of, and induces apoptosis in, the hct116 colon cancer cell line. Mol Med Rep *12(5)*: 7538-7544, 2015. PMID: 26459740. DOI: 10.3892/mmr.2015.4383

126 Endo Y, Ishiwata-Endo H and Yamada KM: Cell adhesion to anosmin *via* alpha5beta1, alpha4beta1, and alpha9beta1 integrins. Cell Adh Migr *12(2)*: 93-100, 2018. PMID: 27715389. DOI: 10.1080/19336918.2016.1221568

127 Theocharis AD and Karamanos NK: Proteoglycans remodeling in cancer: Underlying molecular mechanisms. Matrix Biol *75-76:* 220-259, 2019. PMID: 29128506. DOI: 10.1016/j.matbio.2017.10.008

128 Dos Reis DC, Damasceno KA, de Campos CB, Veloso ES, Pegas GRA, Kraemer LR, Rodrigues MA, Mattos MS, Gomes DA, Campos PP, Ferreira E, Russo RC and Cassali GD: Versican and tumor-associated macrophages promotes tumor progression and metastasis in canine and murine models of breast carcinoma. Front Oncol *9:* 577, 2019. PMID: 31334111. DOI: 10.3389/fonc.2019.00577

129 Hart ML, Rusch E, Kaupp M, Nieselt K and Aicher WK: Expression of desmoglein 2, desmocollin 3 and plakophilin 2 in placenta and bone marrow-derived mesenchymal stromal cells. Stem Cell Rev Rep *13(2)*: 258-266, 2017. PMID: 28154962. DOI: 10.1007/s12015-016-9710-4

130 Rotzer V, Hartlieb E, Winkler J, Walter E, Schlipp A, Sardy M, Spindler V and Waschke J: Desmoglein 3-dependent signaling regulates keratinocyte migration and wound healing. J Invest Dermatol *136(1)*: 301-310, 2016. PMID: 26763450. DOI: 10.1038/JID.2015.380

131 Kamioka H, Tomono T, Fujita A, Onozato R, Iijima M, Tsuchida S, Arai T, Fujita Y, Zhang X, Yano K and Ogihara T: Moesin-mediated p-glycoprotein activation during snail-induced epithelial-mesenchymal transition in lung cancer cells. J Pharm Sci, 2020. PMID: 32173323. DOI: 10.1016/j.xphs.2020.03.008

132 Yu L, Zhao L, Wu H, Zhao H, Yu Z, He M, Jin F and Wei M: Moesin is an independent prognostic marker for er-positive breast cancer. Oncol Lett *17(2)*: 1921-1933, 2019. PMID: 30675256. DOI: 10.3892/ol.2018.9799

Received May 26, 2020
Revised June 14, 2020
Accepted June 26, 2020